The Basics

Paul A. Bottomley

Johns Hopkins University, Baltimore, MD, USA

The basic elements of NMR and its subspecialty magnetic resonance spectroscopy (MRS) are presented at a graduate course level, for the purpose of providing a background to common concepts in chapters that follow. Nuclei eligible for NMR have an odd number of either protons or neutrons, which endows them with a quantum mechanical magnetic moment. When placed in a magnetic field (B_0), such nuclei align and precess about B_0 at discrete quantized orientations and resonant frequencies. Flips between orientations result in radio frequency (RF) emissions and absorptions at the resonant frequency. These transitions can be excited by a circularly polarized RF field (B_1) perpendicular to B_0, and detected as an RF voltage using a tuned RF coil. The NMR signal decays with characteristic time constants T_1 and T_2 that can be measured using various sequences of B_1 pulses. The T_1 and T_2 relaxation times are properties of the molecular-level motion at the nuclei, and form the basis of tissue contrast in NMR imaging. Furthermore, intramolecular variations in the local B_0 due to the presence of chemical bonds produces characteristic shifts of parts-per-million in the NMR frequencies of subgroups of magnetically equivalent nuclei, or moieties. These chemical shifts allow identification of specific biochemicals in MRS experiments employing the Fourier transform of the decaying NMR time signal. The signals from chemically shifted moieties may be enhanced or suppressed by decoupling, Overhauser enhancement, and solvent suppression techniques. The moiety's concentration and volume, B_0, and the NMR receiver's performance are key determinants of the signal-to-noise ratio (SNR), currently limiting detection to about 10^{-6} of the ^{1}H signal from water. Because the NMR signal $\propto B_0{}^2$ and the noise $\propto B_0$ if sample noise is dominant or $\sqrt{B_0}$ if coil noise dominates, the SNR$\propto B_0{}^1$ or $B_0{}^{1.75}$.

Keywords: NMR, relaxation, Bloch equations, chemical shift, spin–spin coupling, water suppression, signal-to-noise ratio

How to cite this article:
eMagRes, 2015, Vol 4: 505–524. DOI 10.1002/9780470034590.emrstm1485

Nuclear Magnetic Resonance

Eligible Nuclei

The NMR phenomenon is exhibited by atomic nuclei with an odd number of either protons or neutrons. This includes, for example, neutrons, protons or hydrogen nuclei (^{1}H), deuterons (^{2}H), carbon-13 (^{13}C), nitrogen-14 and -15, and oxygen-17 (O^{17}), but not unfortunately the more abundant ^{12}C or ^{16}O (Table 1). The NMR nuclei possess quantum mechanical spin angular momentum that endows them with a tiny magnetic field or dipole moment whose strength is characterized by a magnetic moment, μ, that is unique to each nucleus. The spin angular momentum has a quantum number, I, that can have values of $\frac{1}{2}$, 1, 3/2, 2, 5/2, etc., depending on the nucleus. When placed in an applied magnetic field, $\mathbf{B_0}$, a weak torque is exerted on the nuclear magnetic moment, which tends to align it, but because the spin is quantized, only certain orientations of the moment with $\mathbf{B_0}$ are allowed. The number of available orientations is $2(I+1)$, and they are symmetrically oriented about the direction of $\mathbf{B_0}$, which by convention is always chosen as the z-axis of a Cartesian coordinate system (Figure 1).

Because each allowed orientation of the nuclear magnet is more or less favorably disposed relative to $\mathbf{B_0}$, each is associated with a different energy level. The lowest energy levels correspond to orientations that are most closely aligned with $\mathbf{B_0}$, and the highest energy states are aligned against $\mathbf{B_0}$. Transitions between energy levels correspond to jumps between the allowed orientations. These require the emission or absorption of energy quanta in accordance with the Planck relation for the energy difference, $E = h\nu_0$, where h is Planck's constant ($=6.626 \times 10^{-34}$ Js) and we introduce ν_0 as the NMR frequency (Figure 1). This is the frequency at which nuclear magnets rotate or 'precess'† about $\mathbf{B_0}$ at its allowed orientation with the z-axis. In addition to being proportional to ν_0, the energy difference, whose existence is due to the presence of both the nuclear magnet and $\mathbf{B_0}$, is in fact proportional to the magnitude of $\mathbf{B_0}$, denoted B_0. These two proportionalities are combined in the Larmor equation:

$$\omega_0 = \gamma B_0 \tag{1}$$

where $\omega_0 = 2\pi\nu_0$ is the angular NMR frequency (in rad/s) and γ the proportionality constant called the 'gyromagnetic' ratio. Equation (1) is the key to NMR, nuclear magnetic resonance spectroscopy (MRS), MRI, and all of the spatial localization methods used in these endeavors. The gyromagnetic ratio is different for each NMR isotope, and for practical B_0 values of 0.1–10 tesla (T), ν_0 falls in the radio frequency (RF) band: about 0.5–450 MHz. These two facts allow, in principle, each nucleus to be tuned in for NMR, like tuning a radio station on the FM (frequency modulation) band.

†Quotation marks define common NMR terms at first usage, throughout.

Table 1. NMR properties and relative signal-to-noise ratios (SNRs) in muscle tissue at constant B_0 for some common elements[a]

Nucleus	Spin, I	Isotopic abundance (%)	ν_0 (MHz) at $B_0 = 1$ T	SNR/mole of NMR nucleus[a] vs ^{1}H	Elemental concentration in muscle,[b] mmol g^{-1} wet wt	Relative SNR vs ^{1}H in muscle[c]
^{1}H	1/2	99.98	42.577	1	99.21	1
^{2}H	1	0.0156	6.536	0.0628	99.21	9.81×10^{-6}
^{13}C	1/2	1.108	10.705	0.0632	8.920	6.3×10^{-5}
^{14}N	1	99.64	3.076	0.0139	1.963	2.75×10^{-4}
^{17}O	5/2	0.037	5.772	0.2144	46.88	3.75×10^{-5}
^{31}P	1/2	100	17.235	0.1639	0.058	9.52×10^{-5}

[a]Assumes SNR varies linearly with B_0 (SNR$\propto\gamma^2 I[I+1]$), that nuclei are 100% NMR visible and monochromatic, no polarization enhancement, equilibrium, and a noiseless receiver with the same bandwidth (BW; see section titled 'The Intrinsic SNR'). Note that SNR differs from 'NMR sensitivity' ($\propto\gamma^3\, I[I+1]$) reported variously. Relative SNRs are consistent with relative magnetizations at 1 T in Ref. 1 (p. 309), and equation (30) in the section titled 'Calculation of SNR' divided by $\nu_n \propto \omega_0$, to account for frequency-dependent sample noise.
[b]Assumes elemental contents and wet weights for human tissue in Ref. 2.
[c]SNR/mol of nucleus scaled by isotopic abundance and elemental concentration in muscle.

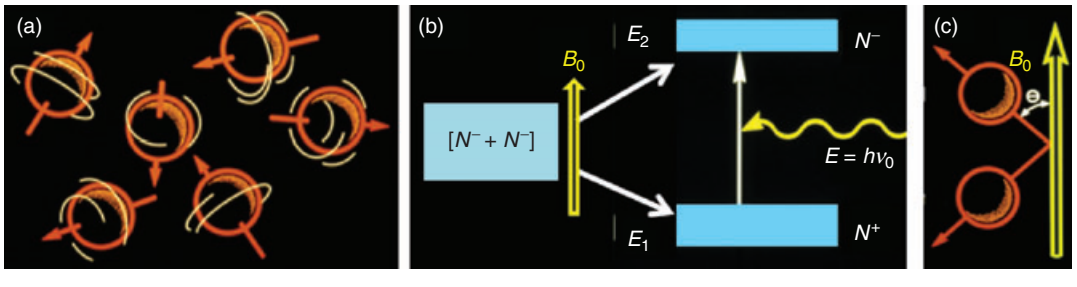

Figure 1. Exposing a population of nuclear spin magnets (a) to a magnetic field $\mathbf{B_0}$ causes the nuclear spin energy to split into two or more levels, E_1 E_2, etc., separated by $E \propto B_0$ (b). The levels are populated according to Maxwell–Boltzmann statistics and the available thermal energy of the lattice. There is a slight excess (N^+/N^-) in the lowest energy state because more nuclei are aligned with $\mathbf{B_0}$ than against it. The orientations of the nuclei relative to $\mathbf{B_0}$ are quantized into $2(I+1) = 2$ levels for spin $I = 1/2$ nuclei such as ^{1}H or ^{31}P (c). Transitions between energy levels and orientations result in emission or absorption of energy at the resonant frequency, ν_0, with a characteristic transition rate $1/T_1$. The widths of E_1 and E_2 are broadened by variations in the local field characterized by rates $1/T_2$ or $1/T_2{}^*$

However, NMR is not performed on a single nuclear spin, but typically on vast numbers of them. The nuclear spin density for a pure substance with formula weight FW is $[n_m A_0/\mathrm{FW}]$ per gram, where A_0 is Avogadro's number (6.02×10^{23}) and n_m the number of NMR nuclei on each molecule of the substance. For example, a 1 ml or 1 g sample of water with FW = 18 and $n_m = 2$ hydrogen nuclei contains about $N_{ml} = 6.7 \times 10^{22}$ nuclei that are eligible for ^{1}H NMR. Biological tissue is about two-thirds water but the other one-third also contains ^{1}H at a comparable density, so there are about 6×10^{22} ^{1}H nuclei in 1 g of tissue as well.

It is fortunate from a safety perspective that when all these nuclei in a living sample are placed in a $\mathbf{B_0}$ field at a temperature of $T = 37\,^\circ$C, they do not all suddenly align, lest there be some dire physiological response. In fact, the thermal motion present in the nuclear spin environment or 'lattice' is much greater than the alignment torque. The $2(I+1)$ energy levels arising from the combined effect of $\mathbf{B_0}$ and the quantized spin angular momentum are populated by all the nuclei in accordance with Maxwell–Boltzmann statistics. For a spin $I = 1/2$ nucleus such as ^{1}H with two orientations (Figure 1c), the excess of spins aligned with a $\mathbf{B_0}$ of 1 tesla (T) instead of against it is only

$$<N^+/N^->\; = \exp(E/KT) = \exp(h\nu_0/KT) \approx \text{seven in a million}$$

where K is Boltzmann's constant and T is in Kelvin. Nevertheless, this leaves a total excess of $\mathbf{B_0}$-aligned nuclear magnets in the 1 ml water of $7N_{ml}//10^6 \sim 5 \times 10^{17}$.

Exciting Resonance

The collective effect of this many nuclei aligning with $\mathbf{B_0}$ is to create a weak net or 'bulk nuclear magnetization', $\mathbf{M}$, proportional to $\mathbf{B_0}$ with magnitude $M = \{N_{ml}.\mu.<N^+/N^->\}$ per milliliter. At equilibrium, $\mathbf{M}$ is aligned with $\mathbf{B_0}$ and denoted M_0 $\hat{\mathbf{z}}$, where $\hat{\mathbf{z}}$ is a unit vector in the z-direction (Figure 2a). Because the spins are precessing with random coherence and jostled by thermal motion, there is no net 'transverse magnetization', $\mathbf{M_{xy}}$, in the x–y plane in which the nuclear spins precess. This means that no actual resonance is observed – just the slight increase in sample magnetization. To see a NMR, $\mathbf{M}$ must be perturbed away from equilibrium. This is equivalent to requiring that the population distribution of the nuclear energy levels be disrupted, after which $\mathbf{M}$ might be observed as it returns or 'relaxes' back to $\mathbf{B_0}$ and the population distribution returns

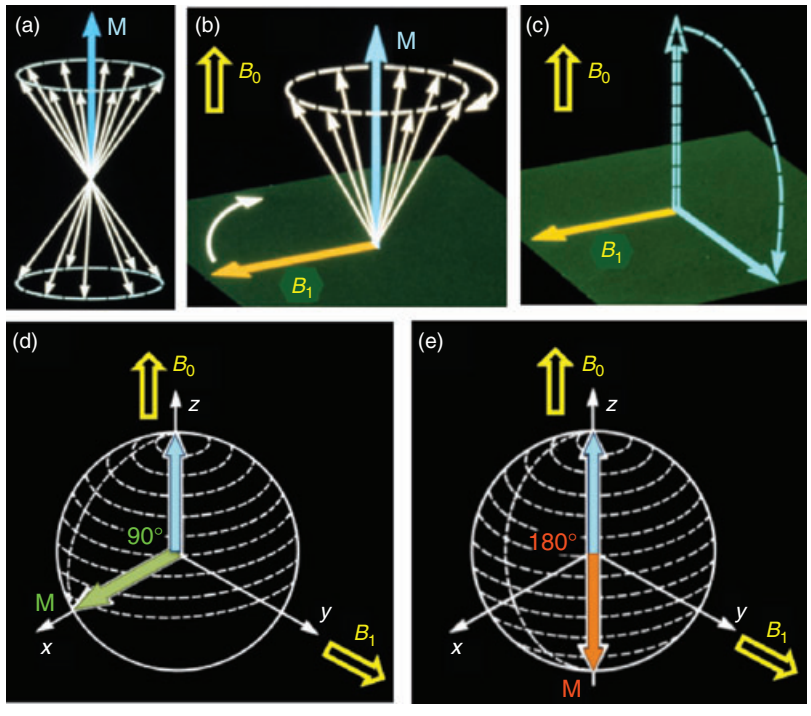

Figure 2. At equilibrium, nuclei precessing about $\mathbf{B_0}$ produce a net longitudinal magnetization, **M**, aligned with $\mathbf{B_0}$, but they are out of phase so there is no net transverse magnetization (a). Application of a transverse RF field, $\mathbf{B_1}$, tuned to ν_o rotates **M** into the transverse plane (b and c). The trajectory of **M** is a spiral rotating about $\mathbf{B_0}$ at ν_o (d and e). If $\mathbf{B_1}$ is turned off when **M** crosses the x–y plane, the B_1-pulse is called a 90° pulse (d). If it is turned off when **M** is inverted, it is a 180° pulse (e)

to thermal equilibrium. To perturb **M** away from $\mathbf{B_0}$ would normally require exerting a torque on **M** of comparable magnitude to that provided by $\mathbf{B_0}$ in say a transverse or minus-$\mathbf{B_0}$ direction, which would be impractical. Instead, a much smaller magnetic field, $\mathbf{B_1}$, can be used to tip **M** if it is precisely tuned to the NMR frequency, ν_0, satisfying equation (1) (Figure 2b). This is analogous to a pendulum whose swing can be increased to extreme levels with the slightest force applied at the pendulum's resonant frequency, transverse to the pendulum's axis. Similarly, $\mathbf{B_1}$ must be applied in the x–y plane because applying it in the z-direction will not perturb **M** away from $\mathbf{B_0}$.

The first NMR on condensed matter[3,4] and indeed the first MRI[5] were performed by 'continuous wave (c.w.)' NMR wherein the B_0 field was swept over a tiny range about the value satisfying equation (1), while a transverse $\mathbf{B_1}$ was applied continuously at the NMR frequency, ν_0: sweeping B_0 was less technically difficult[3] than sweeping the frequency, ν. At resonance, transitions between energy levels are induced, resulting in a net absorption of energy and the first 'NMR spectrum' (Figure 3)[4] or plot of the NMR signal as a function of frequency or equivalently – in light of equation (1) – field strength.

The c.w. method generated the spectrum one point at a time, and is now passé. It was replaced by much more efficient pulsed NMR methods that were introduced a few years after c.w. NMR.[6] Pulsed NMR can excite and measure a whole spectrum (or spatial MRI projection of a sample) at once. In pulsed NMR, $\mathbf{B_1}$ is applied as an RF pulse tuned to ν_0. Its amplitude, although tiny (typically 5–100 μT) compared to B_0, nudges **M** away from the z-axis down into the x–y plane over many cycles, by virtue of being resonant (Figure 2c). The trajectory of **M** is actually a spiral at the resonant frequency (Figure 2d): a 20 μs pulse applied at 42.577 MHz for ^{1}H at $B_0 = 1$ T, for example, would undergo $(20 \times 42.577) = 852$ revolutions. The trick is to turn off $\mathbf{B_1}$ when **M** is precisely at some desirable point in its 3-D vector space.

If you start with M_0 aligned with the $+z$-axis and turn off B_1 exactly when it intersects the x–y plane, you have rotated **M** by a 'flip-angle (FA)' of $\alpha = 90^\circ$ (Figure 2d). At this time, you have the maximum nuclear magnetization vector precessing, rotating coherently, or 'resonating' at ν_0 in the transverse plane. With B_1 now off, the rotating magnet can induce a voltage or 'NMR signal' in a pick-up coil that is tuned to ν_0 and is sensitive to the transverse field (Figure 4a). The pulse whose duration and amplitude first generate the maximum NMR signal following a period of equilibration is deemed to be a '90° or π/2 NMR pulse'.

If B_1 is left on after M_0 passes through 90°, the magnetization will keep going until it is fully inverted (Figure 2e). At this point, the transverse magnetization is minimal, as is the NMR signal induced in the coil. This defines a '180°' or 'π NMR pulse'. If B_1 has the same amplitude profile as the 90° pulse, the 180° pulse is exactly twice the duration of the 90° pulse. While 90° and 180° pulses are often applied sequentially as 'pulse sequences' in NMR and MRI, other arbitrary FAs are certainly allowed and used. As minima can be easier to detect than maxima, determining the 180° pulse length from the first signal minimum following a maximum is often the easier way to calibrate FA in practice. The relation between an FA of α

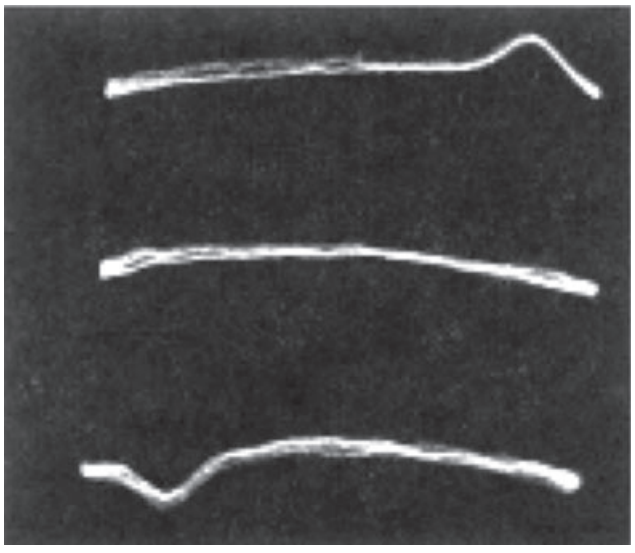

Figure 3. Oscilloscope trace depicting one of the first NMR spectra – from water.[4] The field is cycled at 60 Hz through the resonance at $B_0 = 0.183$ T with the field slightly higher (top) and lower (bottom) than the resonance. In the central trace, the field sweep was centered on the resonance, saturating it. (Reprinted figure with permission from F. Bloch, W. W. Hansen, and M. Packard, Phys. Rev., 69, 127, 1946. Copyright 1946 by the American Physical Society. DOI: http://dx.doi.org/10.1103/PhysRev.70.474)

radians B_1 (tesla) and pulse length τ (sec) derives directly from equation (1) with B_1 substituted for B_0:

$$\alpha = \gamma B_1 \tau \qquad (2)$$

This reflects the fact that in a frame-of-reference rotating at exactly the NMR frequency about the z-axis, the spiral trajectory of **M** during the pulse vanishes, and the effective field is equal to B_1. In this 'rotating frame of reference', B_1 appears static and directed along say the x-axis of the rotating transverse plane. Thus, when B_1 is turned on, M will precess or 'nutate' directly about B_1, traversing an arc of α (Figure 2c). The transverse component is simply $M_{xy} = M \sin \alpha$.

The pick-up coil that detects the RF voltage induced by M_{xy} can be the same one used to generate B_1, or a separate tuned NMR receiver coil. The coil is connected to an NMR spectrometer or MRI scanner. There, the tiny NMR signal is first amplified, and then 'demodulated' by removing the ν_0 component (see ***Magnetic Resonance Spectroscopy Instrumentation***). This brings the NMR signal essentially into an audio frequency range for display and processing. Such processing is analogous to the demodulation that an FM radio performs on an 88.1 MHz radio signal from Baltimore station WYPR say to enable us to listen to the sound. On an NMR radio tuned to ν_0, we listen to the rotating frame directly.

Relaxation

T_1 and T_2

The NMR signal excited by the $\alpha \neq \pi$ NMR pulse is called a 'free induction decay' or 'FID' (Figure 4c). The decay in M_{xy} is due to two distinct processes. First, M_{xy} decays owing to the dephasing of nuclear spins in the sample owing to tiny differences in the local B_0 magnetic field, which affect the local NMR frequency via equation (1). This dephasing can have both intrinsic and external or instrumental origins, which are respectively irreversible or reversible using NMR methods described in the following text. Generally, the FID is assumed to be a mixture of both components, and the decay is deemed to have a time constant 'T_2* (T_2-star)', which is assumed to be exponential whether it is or not. The most common instrumental contributor to T_2* is inhomogeneity in B_0 due to gradients, metal, eddy currents, etc. The irreversible part of the decay is characterized by a time constant 'T_2' (no asterisk), called the 'transverse relaxation time' or the 'spin–spin relaxation time'. T_2 decay results from irreversible dephasing owing to the presence of local gradients at the molecular level arising from both static and mobile molecular-level sources.[6–9]

Second, if the M_{xy} dephasing processes do not dominate, **M** must eventually relax back to the z-axis to align with $\mathbf{B_0}$ (Figure 1b). The growth in the z-magnetization, M_z, is characterized by a time constant 'T_1', called the 'longitudinal' or 'spin–lattice relaxation time'. T_1 relaxation is facilitated by the presence of variations in the local magnetic field at ν_0 and $2\nu_0$, such as those caused by inter- and intramolecular motions of nearby nuclear dipoles. Just like B_1, these local field fluctuations at the NMR frequency facilitate the transitions between energy levels that are necessary to restore the equilibrium state.[7,8]

Expressions for T_1 and T_2 due to dipole–dipole interactions are[8]:

$$\frac{1}{T_1} = \frac{3}{2}\gamma^4 \bar{h}^2 I(I+1)[J_1(\nu_0) + J_2(2\nu_0)] \qquad (3)$$

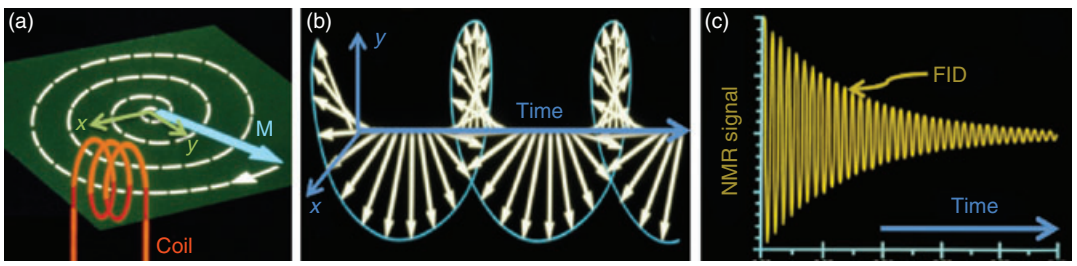

Figure 4. The magnetization rotating in the x–y plane generates an RF voltage in a tuned pick-up coil sensitive to the transverse field (a). The amplitude of the rotating magnetization (b), and the induced voltage (c) decay with a time constant T_2 or T_2*, producing a free induction decay (FID)

and

$$\frac{1}{T_2} = \gamma^4 \overline{h}^2 I(I+1)\left[\frac{3}{8}J_0(0) + \frac{15}{4}J_1(\nu_0) + \frac{3}{8}J_2(2\nu_0)\right] \quad (4)$$

where $\overline{h} = h/2\pi$ and the J's are the spectral density of motion calculated at ν_0, $2\nu_0$, and static ($\nu = 0$) frequencies. The $2\nu_0$ term arises because motion at twice the frequency can reverse the sense of a spin going the wrong way, inducing a transition.[7] Equation (3) was used to calculate a reasonably accurate T_1 for ^{1}H nuclei (protons) in pure water, based on J's deduced assuming only an isotropic diffusion motion for the protons.[7] Nevertheless, models describing the relaxation times of nuclei in biological tissue remain at best empirical.[9,10]

The T_1 and T_2 values depend on the molecular-level environment, and typically vary with ν_0, temperature, the molecule, the location of the nuclei on the molecule, and in biological applications, the tissue it is in.[9,10] In biological systems ^{1}H, T_1s typically range from 0.1 to 2 s. T_2s are shorter at about 10–300 ms, owing to the added effects of the low-frequency and static processes (the J_0 term), which ensure that T_2 is always less than T_1. Differences between the relaxation times of ^{1}H in water in biological tissue are responsible for image contrast in MRI, and its utility in medicine.[9,10] *The importance of relaxation times to MRI contrast is truly immense, but of even greater importance to the field of NMR as a whole is that they endow the NMR spin system with a memory that lasts several T_1s. Without such memory, stringing together, sequentially, all of the crafty space- and time-encoding methods that make possible just about everything NMR, MRI, and MRS does would not work.*

The Bloch Equations

Generally, an NMR experiment will be comprised of one or more excitations and periods of detection. The resulting magnetization is described by the 'Bloch equations'[11]:

$$\begin{aligned}
\frac{dM_x(t)}{dt} &= \gamma(M_y(t)B_z(t) - M_z(t)B_y(t)) - \frac{M_x(t)}{T_2} \\
\frac{dM_y(t)}{dt} &= \gamma(M_z(t)B_x(t) - M_x(t)B_z(t)) - \frac{M_y(t)}{T_2} \\
\frac{dM_z(t)}{dt} &= \gamma(M_x(t)B_y(t) - M_y(t)B_x(t)) - \frac{M_z(t) - M_0}{T_1}
\end{aligned} \quad (5)$$

The first bracketed terms on the right describe in component form, the nutation of $\mathbf{M}$ from the torque imparted by the $\mathbf{B}$ field during excitation. This derives from the vector cross product, $d\mathbf{M}(t)/dt = \gamma\mathbf{M}(t) \times \mathbf{B}(t)$. The subtracted quotients describe the decay in the transverse magnetization at a rate $1/T_2$, and the growth in longitudinal magnetization at $1/T_1$. These equations permit numerical simulation of any NMR experiment by breaking the differential terms on the left into tiny steps, ΔM_x, Δt, etc. Usually, the pulse length $\tau \ll T_1$, so the T_1 and T_2 terms can be neglected during pulses while the $\mathbf{B_1}$ terms vanish between pulses.

Circular Polarization of B_1. Importantly, the nuclei only rotate or precess in one direction relative to $\mathbf{B_0}$ or $\mathbf{B_1}$ (Figures 2 and 4). This means that the RF signal that is emitted or absorbed during NMR is circularly polarized, which has two practical consequences. First, only the circularly polarized component of $\mathbf{B_1}$ rotating in the same direction as the spins can excite NMR. Before the mid-1980s, $\mathbf{B_1}$ was generated in a single transverse direction, the x-axis in the laboratory frame-of-reference say, by applying a sinusoidal current, $I\cos\omega t$, to a loop coil (such as a solenoid, a 'saddle', a 'figure-8', or surface coils) in a configuration that is now referred to as 'linear excitation'. The sinusoidal current only produces a sinusoidal B_1 which is not circularly polarized. This nevertheless works because the linear field can be decomposed into two counter-rotating fields:

$$\begin{aligned}
B_1\hat{\mathbf{x}} = B_{10}\cos\omega t \cdot \hat{\mathbf{x}} &= (B_{10}/2)(\cos\omega t \cdot \hat{\mathbf{x}} + \sin\omega t \cdot \hat{\mathbf{y}}) \\
&+ (B_{10}/2)(\cos\omega t \cdot \hat{\mathbf{x}} - \sin\omega t \cdot \hat{\mathbf{y}})
\end{aligned} \quad (6)$$

where $\hat{\mathbf{x}}$ and $\hat{\mathbf{y}}$ are unit vectors in the x- and y-directions and B_{10} is the amplitude of $\mathbf{B_1}$. The cost of creating this virtual circularly polarized field is that only half the B_1 is being used to excite NMR: the other half is wasted on the counter-rotating component. Given that $B_1 \propto$ current, I, in the excitation coil and power $\propto I^2$, the difference in the peak RF power required to produce B_{10} vs $B_{10}/2$ is a factor of 4.

By the mid-1980s, linear excitation for head and whole body NMR was replaced by circularly polarized excitation, primarily as a consequence of the invention of the 'birdcage' coil for MRI.[12] Circular polarization is achieved by applying two sinusoidal waves, 90° out of phase, to two 'quadrature' ports that are both physically and electromagnetically displaced by 90° (or a 1/4-wavelength) around the coil. The excitation field is then just

$$\mathbf{B_1} = B_{10}(\cos\omega t \cdot \hat{\mathbf{x}} + \sin\omega t \cdot \hat{\mathbf{y}}) \quad (7)$$

This configuration cuts the peak power requirement fourfold. However, the total average power input and the total power deposited in the sample are only halved because power must now be applied to two ports instead of the one.[12] The circular polarization of the NMR signal can be verified by interchanging the two quadrature inputs: no NMR occurs with the inputs backwards, except at locations where the circular polarization is imperfect.[12]

The second consequence of the rotating field relates to the 'signal-to-noise ratio' (SNR) of the NMR signal.[13,14] Here the 'signal' is the NMR voltage induced in the detector coil. The 'noise' voltage, ν_n, is measured as the 'root-mean-square' (r.m.s.) of what is left over when the NMR signal has decayed away. Even though the NMR signal rotates in only one direction, a linear detector is sensitive to both counter-rotating components and therefore detects the noise voltage from both components, ν_{n0° and ν_{n90°. Because ν_{n0° and ν_{n90° are uncorrelated, the r.m.s noise adds as $\sqrt{(\nu_{n0^\circ}{}^2 + \nu_{n90^\circ}{}^2)} = \nu_n\sqrt{2} \approx 1.4\nu_n$. Thus, using a linear detector carries a 40% SNR penalty compared to a true quadrature detector sensitive only to the rotating component.[14]

Measuring Relaxation

T_1 and Partial Saturation. The simplest NMR pulse sequence just involves applying an α° FA pulse of duration $\tau \ll T_1$, and acquiring the excited signal. Some 'repetition period', TR, is waited before the α° pulse is applied again. After the first pulse, M_0 is rotated α° into the x–y plane and begins to precess at ω_0 about the z-axis (Figure 5a). According to the solution of equation (5) with the pulse off, the M_z component starts with magnitude $M_0 \cos\alpha$ and begins to grow back to M_0 at a rate of T_1. It is convenient to represent the transverse component as a single rotating vector $\mathbf{M_{xy}}$. It starts with magnitude $M_0 \sin\alpha$ and decays with time constant $T_2{}^*$. Thus:

$$M_{xy}(t,\ T_2{}^*) = M_0 \sin\alpha \cdot \exp(-t/T_2{}^*)$$

and

$$M_z(t,\ T_1) = M_0 \cos\alpha \cdot [1 - \exp(-t/T_1)] \qquad (8)$$

If this sequence is repeated with a TR comparable to T_1 and if M_{xy} dephases irreversibly between pulses, a 'steady state' is reached at which point M_{xy} after the pulse is equal to M_z immediately before the pulse (Figure 5b). The NMR signal decreases to

$$\frac{M_{xy}}{M_0} = \frac{[1 - \exp(-\mathrm{TR}/T_1)]\sin\alpha}{1 - \cos\alpha \cdot \exp(-\mathrm{TR}/T_1)} \exp(-t/T_2{}^*) \qquad (9)$$

which includes the $T_2{}^*$ decay measured at time t relative to the last NMR pulse. The maximum NMR signal per unit time occurs at the so-called 'Ernst angle' given by

$$\cos\alpha_E = \exp(-\mathrm{TR}/T_1), \text{ at which point} \qquad (10)$$

$$\frac{M_{xy}}{M_0} = \sqrt{\frac{1 - \exp(-\mathrm{TR}/T_1)}{1 + \exp(-\mathrm{TR}/T_1)}} \exp(-t/T_2{}^*) \qquad (11)$$

Equation (9) shows that if the simple α° pulse sequence is repeated with different values of TR, the signal measured at steady state will be dependent on T_1, which can be determined therefrom. In particular, when $\alpha = 90^\circ$, the transverse magnetization has an initial amplitude

$$M_{xy}/M_0 = [1 - \exp(-\mathrm{TR}/T_1)] \qquad (12)$$

In practice, the prudent course of analysis is to perform a three-parameter fit to the signal

$$S = P - Q \cdot \exp(-\mathrm{TR}/T_1) \qquad (13)$$

with P, Q, and TR as fitting constants, to compensate in part for the ill effects of B_1 inhomogeneity on FA. Because S declines or 'saturates' as TR is decreased because the spin population has insufficient time to equilibrate, this method of measuring T_1 is known as the *partial saturation (PS) method*. Note that the signal is considered completely 'saturated' when the population of spins occupying all of the nuclear magnetic energy levels are identical.

T_1 and Inversion Recovery. Adding pulses with different FAs adds complexity, especially for $\alpha \neq 90^\circ$ or $\alpha \neq 180^\circ$ and for short TRs, because the accumulated effect of all excitations applied within the spin memory of several T_1 periods must be accounted for. The special case of the 'inversion recovery (IR) method' starts with the magnetization at equilibrium, $M_0\hat{\mathbf{z}}$, directed along the z-axis with unit vector $\hat{\mathbf{z}}$. A 180° 'inversion pulse' is applied, which inverts the longitudinal magnetization to $\{-M_0\hat{\mathbf{z}}\}$. This generates no transverse magnetization ($M_{xy} = 0$) and therefore no NMR signal. Nevertheless, the longitudinal magnetization begins to shrink from $\{-M_0\hat{\mathbf{z}}\}$ and grows back along the z-axis toward equilibrium. Then, at some 'inversion time', TI, after the 180° pulse, a 90° pulse is applied

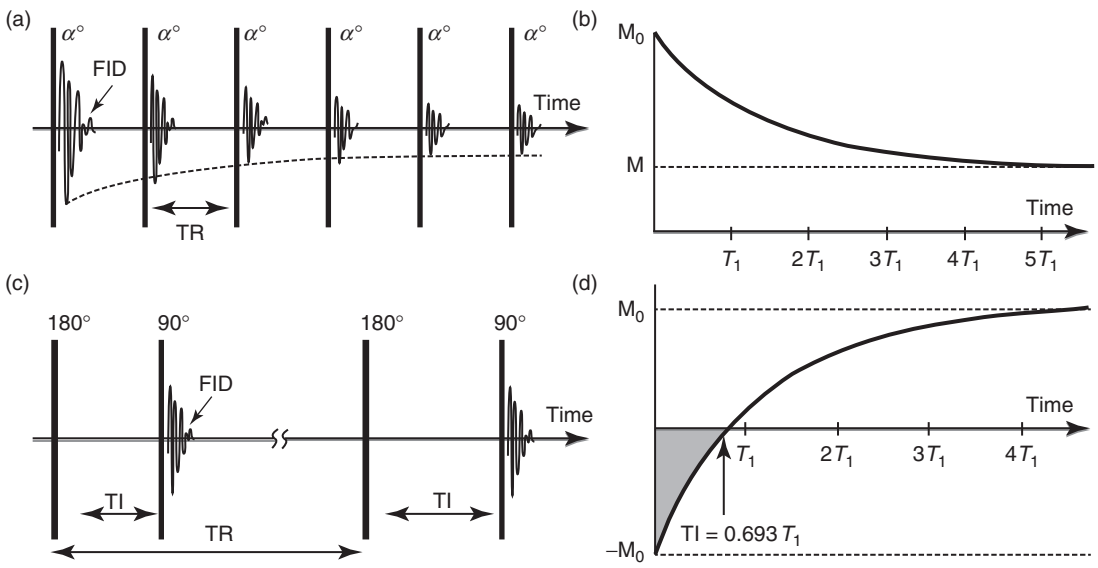

Figure 5. The effect of applying an RF pulse sequence comprised of a series of FA = α° pulses with period TR $\ll T_1$ (a) is to partially saturate the NMR signal, which declines to a steady-state value after several T_1s given by equation (9) (b). When $\alpha = 90^\circ$, the steady-state value is $M_0(1-\exp \mathrm{TR}/T_1)$, per equation (12). Inversion recovery (IR) comprises a 180°–TI–90° sequence repeated at TR $\gg T_1$ (c). The magnetization is initially inverted and negative for TI < 0.69 T_1, zero at TI = 0.69 T_1, and positive for TI > 0.69 T_1, spanning the range $\pm M_0$ (d)

(Figure 5c). This flips the residual shrinking/growing M_z component into the x–y plane. The signal immediately following the 90° pulse (with the T_2* term omitted) is:

$$M_{xy} = M_0[1-2\exp(-TI/T_1)] \qquad (14)$$

Repeating this sequence with a set of different TI values yields an exponential curve from which T_1 can be obtained from signals measured at the same time t relative to the last (90°) pulse (Figure 5d).

Again, it is prudent to fit the data to an equation of the form of equation (13), replacing TR by TI. The IR method is advantageous over PS in that it provides twice the dynamic range of signal dependence on T_1. A disadvantage is that equation (14) is only valid when starting from equilibrium: repeat applications of the sequence require a delay of TR $\gg T_1$, which reduces its efficiency for signal averaging or spatial localization. Note also that in the special case when

$$\exp(-TI/T_1) = 1/2, \text{ i.e., } TI = 0.693\ T_1 \qquad (15)$$

Equation (14) shows that M_{xy} passes through zero. At this point, T_1 can be obtained directly from a single determination of the TI that yields zero signal from an IR experiment, using equation (15). This is known as the *T_1-null* method.

T_2 and Spin-Echoes. The distinction between T_2 from T_2* is whether the decay in M_{xy} is facilitated by intrinsic molecular-level interactions or by other external instrumental factors. Of the latter, the primary culprit is static magnetic field inhomogeneity. Such dephasing can be reversed by the 'Hahn spin-echo (SE)' experiment.[6] The SE experiment also employs 90° and 180° pulses, but in reverse order to IR (Figure 6a). Starting with the nuclei at equilibrium, the first 90° pulse flips M_0 into the transverse (x–y) plane, where it begins to decay at T_2*. Nuclei in different locations in the sample dephase owing to local differences in B_0 arising from the inhomogeneity and equation (1). However, even though the observed signal may have completely dephased to zero, nuclei at different locations in the sample may still precess coherently about $B_0\hat{\mathbf{z}}$ at their own Larmor frequencies, as yet unaffected by the intrinsic spin–spin (T_2) relaxation processes.

Application of a 180° inversion pulse at time TE/2 following the 90° pulse inverts all of the spins in the x–y plane: they remain in the x–y plane, but their relative phases are now reversed (Figure 6b). The B_0 inhomogeneity that caused the dephasing is unchanged, so the phases of the nuclei continue to evolve at the same rates. However, now as a consequence of the phase reversal imparted by the 180° pulse, the continued phase evolution brings the nuclei back into phase, producing a 'SE' at time TE.[6] The echo signal waxes and wanes with time constant T_2*, but the signal at the center of the echo is decreased relative to the signal immediately following the initial 90° pulse, by only the intrinsic T_2, plus the effects of translational diffusion.[6,15] The latter arises because echo formation does not compensate for the effects of spins moving to a slightly different B_0 during TE. A plot of the maximum echo-height measured after repeating the experiment with a series of different TE values is – according to equation (5) – exponential with time constant T_2.

Echo formation need not end with a single echo. The T_2*-dephased echo can be refocused again and again using a 'Carr–Purcell (CP)' sequence[15] wherein 180° pulses are repeated at intervals of TE following the first 180° pulse, which was applied at time TE/2 after the first 90° pulse (Figure 6c). The echoes form at the center of each TE period, and it can be shown that the mean-square of the phase dispersion due to translational diffusion in a B_0 field with static inhomogeneity is reduced by n_e^2, where n_e is the number of spin echoes in the CP 'echo-train' with TE $\ll T_2$.[15] The peak signal of each echo in the train traces the exponential T_2 decay, so T_2 can be measured

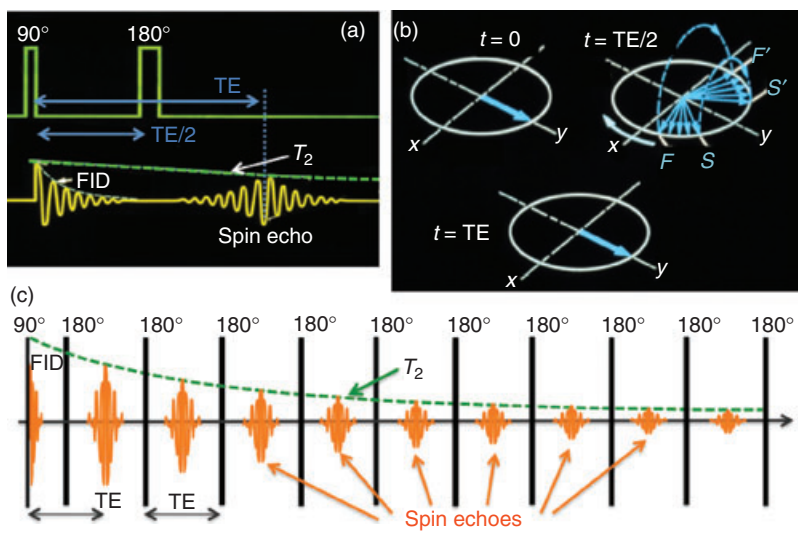

Figure 6. (a) The spin-echo pulse sequence comprises a 90°–TE/2–180° pulse sequence producing a spin-echo at time TE whose peak height is attenuated by T_2. (b) At time $t = 0$, the 90° pulse tips **M** into the x–y plane and the spins begin to dephase owing to T_2* processes. At t = TE/2, the 180° pulse flips over the dephasing spins, but the continued dephasing now brings spins F to S back together to form the echo at t = TE. (c) In the Carr–Purcell sequence, a train of spin-echoes are induced by repeating the 180° pulses at intervals of TE after the first 180° pulse. The height of the echoes traces the T_2 decay

from a single $90^\circ - n_e\{TE/2 - 180^\circ - TE/2\}$ pulse sequence (with n_e = the number of echoes; Figure 6c). However, if the 180° pulses are not perfectly set, errors accumulating during the course of the echo-train cause dephasing that results in the measured T_2 being lower than it should be. This error may be remedied by phase-shifting the B_1 by 90° between the 90° pulse and the subsequent 180° pulses – basically shifting the B_1 field from the x-axis to the y-axis in the rotating frame of reference, say.[16] The effect of the error – the displacement of **M** above or below the x–y plane – remains, but it is not cumulative. This small modification to CP is known as the 'Carr–Purcell–Meiboom–Gill' (CPMG) sequence.[16] The decay in the peak echo height following the ith 180° pulse is thus:

$$M = M_0 \exp(-n_i TE/T_2) \qquad (16)$$

Note that while the SE, CP, and CPMG experiments are designed to overcome the effects of static (B_0) magnetic field inhomogeneity, they are ineffective in dealing with time-dependent inhomogeneities occurring within periods of order T_2, such as those due to eddy currents induced in surrounding metallic structures by MRI or MRS localization gradients, 'unbalanced' spatial localization gradients, temperature, or current variations in the permanent or electromagnets used to generate B_0.

Stimulated Echoes. Spin echoes can actually be stimulated whenever multiple pulses are applied in intervals that are short compared to T_2. For example, when a 90° pulse followed by another 90° pulse at time TE/2, an echo will form at time TE (Figure 7a).[6] This is because after the first 90° pulse, the spins dephase to form a pancake in the x–y plane, which is tipped into the y–z plane by the second 90° pulse (Figure 7b,c). The relative phases of the spins are also inverted, as in the SE method. This pancake has a component equal to half of the magnetization in the x–y plane, which refocuses to form a 'stimulated echo (STE)' (Figure 7d).[6,17] The rest of the signal is in the longitudinal direction, not subject to T_2 relaxation processes, and is not detected. The height of the echo in the x–y plane traces an exponential in TE/T_2 as in the other T_2 methods.

Echoes stimulated in this manner are generally not used to measure T_2 because of their reduced signal vs the SE and CP approaches. However, the sequence is used in MRS and MRI to buy time for other spatial or functional encoding involving the half of the magnetization that is preserved from T_2 decay in the longitudinal direction with its 'spin memory' otherwise intact. The typical application involves a third 90° pulse applied at a 'mixing time, TM' after the second 90° pulse (Figure 7e). During the TM ($\ll T_1$) period, the half of the magnetization comprising the longitudinal components of the pancake is dispersed along the z-axis, quietly relaxing at T_1. Meanwhile, the STE occurring between the second and third 90° pulses from the other half of the magnetization in the transverse plane is ignored or deliberately dephased (see the following text). The third 90° pulse tips all of the remaining longitudinal components into the x–y plane, where they are again subject to T_2 processes resulting in an STE at time TE/2 later. Although in this case, a total time {TE + TM} has elapsed (Figure 7e), the T_2 decay approximates that of the shorter period, TE.

Generally, in order for the STE to derive solely from all three 90° pulses together and not subsets thereof, other spurious NMR signals must be suppressed. For example, in addition to the signal from the longitudinal component preserved during TM and stimulated by all three pulses, there are three FIDs from the three 90° pulses taken individually; then the three STEs from the first and second, the first and third, and the

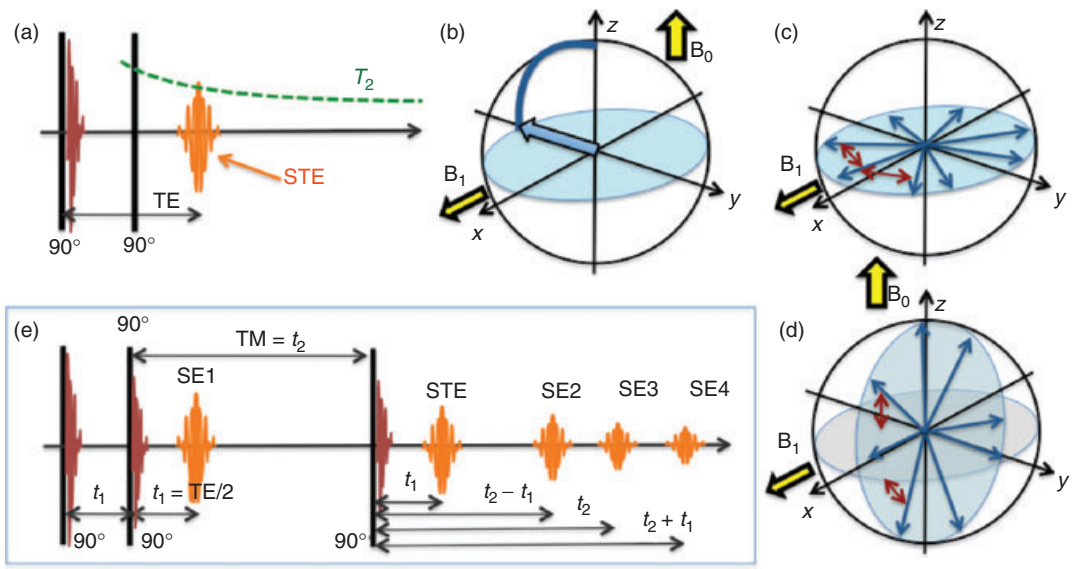

Figure 7. (a) Simple stimulated echo (STE) pulse sequence comprised of two 90°pulses spaced by period TE/2. The STE produced by repeating the sequence with different TEs traces a T_2 curve. (b) The first 90° pulse flips the spins into the x–y plane where they dephase owing to T_2^* processes (c). The second 90° flips the pancake vertically inverting half (d), which refocuses forming the STE. (e) A typical STE sequence used for MRS includes a third 90° at time t_2 = TM after the second. This tips the longitudinal component not included in SE1 into the x–y plane to generate the STE. However, there are four other echoes (SE1–SE4) that are not produced by all three pulses, and are generally not acquired or deliberately dephased. (Adapted from Refs 6 and 17)

second and third pulses; plus an echo from the first STE and the third pulse (Figure 7e).[17] Suppression is generally performed by application of short intense magnetic field gradient 'crusher pulses' applied after each RF pulse gradient.[18] The crusher pulses rapidly dephase the unwanted signals, to vanquish them from the echo time at {TE + TM} at which point the signal is sampled. To ensure that the same dephasing environment (due to the field inhomogeneity imposed by the gradient pulses) is present during the first and second TE/2 periods for correct formation of the STE, the gradient pulses after the first and the third 90° pulses must be identical.

T_2 and Linewidth. While T_1 is a measure of the rate of transitioning between the $2(I+1)$ energy levels that arise from the combined effect of $\mathbf{B_0}$ and the quantized spin angular momentum, T_2 being a measure of the local magnetic field environment reflects the linewidth of the energy levels (Figure 1b). Because the local magnetic field experienced by each spin affects the local NMR frequency, ν_0, via equation (1) and ν_0 is related to energy via $E = h\nu_0$, the linewidth of the resonance in units of B_0, frequency, and energy are all proportionate. If the effects of instrumental B_0 inhomogeneity can be neglected (i.e., $T_2 \ll T_2{}^*$), the linewidth of the NMR signal measured in hertz at 'full-width half-maximum (f.w.h.m.)' in a c.w. NMR experiment is

$$\Delta\nu_0 = 1/(\pi T_2) \tag{17}$$

This relates an exponential decay with time constant T_2 seen by pulsed NMR to the width of the same resonance studied in a c.w. frequency-sweep experiment. The lineshape in c.w. NMR that corresponds to the exponential decay in the pulse experiment is a 'Lorentzian function', which is given by:

$$f_L(\nu, T_2) = \frac{T_2}{1 + \{2\pi(\nu - \nu_0)T_2\}^2} \tag{18}$$

with ν as the sweep frequency. This function peaks at $\nu = \nu_0$. Equation (17) is the solution of equation (18) for $f_L = \pm 1/2$.

Another lineshape often encountered in NMR is 'Gaussian'. This differs from Lorentzian in that it decays faster at the wings of the resonance, or equivalently, as time advances during the FID. This can arise owing to more ordered (lattice-like) interactions between the spins, or more commonly in vivo, owing to instrumental factors such as transient gradients arising from residual eddy currents that are induced in the magnet structure by magnetic field gradient pulses used for spatially localizing the NMR signal. In any case, Gaussian lines have the form:

$$f_G(\nu, T_2) = \exp(-[\nu - \nu_0]^2/2\sigma^2) = \exp(-4\pi[\nu - \nu_0]^2 {T_2}^2) \tag{19}$$

where $\sigma = 1/\{T_2\sqrt{(8\pi)}\}$ is the standard deviation of the Gaussian function. Solving for $f_G = \pm 1/2$ analogous to equation (17) yields an f.w.h.m. for Gaussian lines of:

$$\Delta\nu_0 = \frac{\sqrt{\ln 2/\pi}}{T_2} \tag{20}$$

Even though T_2 can be obtained from linewidth measurements via equations (17) or (20), it is prudent to replace T_2 by $T_2{}^*$ when instrumental contributions are significant or unknown.

Fourier Transform NMR

The healthy ear is accustomed to differentiating the time-dependent audible signals of popular music by their discrete frequencies – bass, mid-range, treble, monotonic drones, whistles, etc. As implied by equations (17–20), the time-dependent NMR signal is intimately related to the frequency spectrum. A single exponentially decaying time-domain NMR signal detected by an FM radio receiver tuned to $\{\nu_0 + 1000\}$ Hz sounds such as a single pure 1 kHz note struck and decaying with a time constant T_2. Its frequency spectrum is a single peak at 1 kHz whose sharpness increases as T_2 (or $T_2{}^*$) lengthens.

The standard method of determining a frequency spectrum from a time signal mathematically (vs the human ear) is the 'Fourier transform (FT)'. The FT fits an interval of time domain, say an NMR acquisition window tAQ, with a mathematical series comprised of a sum of time-dependent sine and cosine waves.[19] The frequencies of the waves are in practice limited to the 'bandwidth (BW)' set by the receiver (analogous to the audible frequency range of hearing). Because the NMR signal is circularly polarized (see section titled 'Circular Polarization of B_1'), it is convenient to represent it by Euler's formula, $\exp(i\omega t) = \cos(\omega t) + i\sin(\omega t)$, with complex 'real' and 'imaginary' components 90° out of phase, and $i = \sqrt{-1}$. The FT is thus generally written in complex form. A plot of the amplitudes of all the sine (and cosine) waves obtained by FT of the complex time-domain signal from the pulsed NMR experiment, arranged as a function of frequency, now constitutes the 'NMR spectrum'. The complex spectrum obtained by FT of the time-domain signal from the pulse experiment is:

$$S(\omega) = \int_{tAQ} s(t)e^{-i\omega t}dt \;\text{ or }\; S(\nu) = \int_{tAQ} s(t)e^{-i2\pi\nu t}dt \tag{21}$$

Moreover, this result is equivalent to the complex (circularly polarized) spectrum measured by c.w. NMR. Conversely, the FT of the frequency-domain signal from the c.w. experiment is:

$$s(t) = \frac{1}{2\pi}\int_{BW} S(\omega)e^{i\omega t}d\omega \;\text{ or }\; s(t) = \int_{BW} S(\nu)e^{i2\pi\nu t}d\nu \tag{22}$$

which is equivalent to the time-domain signal measured by pulsed NMR.

As an example, the real component of the FT of $s(t) = M_{xy}(t, T_2)$ from equation (8) is equal to $S_{Re}(\nu) = f_L(\nu, T_2) \cdot M_0 \sin\alpha$, with f_L defined in equation (18). The corresponding imaginary component is $S_{Im}(\nu) = f_L{}'(\nu, T_2) \cdot M_0 \sin\alpha$, where

$$f_L'(\nu, T_2) = \frac{2\pi(\nu - \nu_0){T_2}^2}{1 + \{2\pi(\nu - \nu_0)T_2\}^2} \tag{23}$$

is the 90° 'out-of-phase' complement of equation (18). By convention, the real, 'in–phase' or pure 'absorption-mode' component of the complex spectrum is taken as that in which the signal is all positive. The 'imaginary', 'quadrature', or 'dispersion-mode' component, being 90° out of phase, has both positive and negative components. In practice, FT often produces an asymmetric mixture of absorption and dispersion modes that must be corrected by adding a phase term (ϕ) to the

exponent (e.g., $\exp\{i\omega t + \phi\}$etc.) when the absorption mode is to be viewed as is customary.

Of course, equations (18–23) also assume a continuous distribution of signal in the time and frequency domains. While a continuous distribution is appropriate for analog detection, NMR signals today are invariably not continuous, but digitally sampled by analog-to-digital converters (ADCs) into N complex data points, a process performed after they have been amplified and demodulated (see section titled 'Exciting Resonance'). FT is then done in a digital computer. In this case, the integrals in equations (21) and (22) are replaced by the corresponding series formed by the digitized data points:

$$S\left(\frac{k}{N\Delta t}\right) = \sum_{n=0}^{N-1} s(n\Delta t)\mathrm{e}^{-i2\pi nk/N} \qquad (24)$$

where Δt is the 'sampling interval' per datum also known as the 'dwell time'; and n and k and integers denoting the nth and kth point in the time and frequency domains, respectively. Equation (24) is known as the *discrete Fourier transform* (*DFT*). Similar series replace the other integrals in equations (21) and (22).

The great advantage of the FT NMR method is that it can acquire an entire spectrum in a single acquisition, whereas the c.w. method must acquire it one point at a time. The upshot is an enormous N-fold efficiency advantage for FT NMR, which can translate to SNR. For example, if the pulse experiment is repeated N-times and the results added to obtain a spectrum in the same time as the point-by-point c.w. experiment, a $\sqrt{N}$-fold SNR advantage results, because the signals add $\propto N$ while the r.m.s. of random noise adds $\propto\sqrt{N}$. This assumes equivalent receiver BW and RF excitations for the two experiments, which may well not be the case. Nevertheless, enormous gains in efficiency and SNR were realized when FT NMR was introduced.[19]

Time-Domain Filtering

So, how long should the acquisition window in the time domain, tAQ, be, and how does it relate to the receiver BW or 'sweep-width' in the c.w. experiment? Because time and frequency are 'conjugate pairs', in the DFT experiment

$$\mathrm{BW} = 1/(\mathrm{tAQ}) = 1/(N\Delta t) \qquad (25)$$

As it takes at least two points in each cycle to define a frequency, the highest frequency that can be digitally sampled and accurately resolved in this interval is $\nu_{\mathrm{Nyq}} = 1/(2\,N\Delta t) = 1/(2\cdot \mathrm{tAQ})$. Thus, BW must at least extend to the range $\pm\nu_{\mathrm{Nyq}}$, where ν_{Nyq} is known as the *Nyquist frequency*. Because the frequency or 'spectral' resolution is inversely proportional to the acquisition window, the spectral resolution increases when tAQ is extended. However, extending tAQ for more than 2.5 times $T_2{}^{\star}$ may add little more than noise, limits TR and TE, and reduces SNR efficiency (SNR per unit time). One trick that is routinely used in MRS is to double or quadruple the time-domain data simply by appending zeros or 'zero-filling' the acquisitions. Noticeable improvements in spectral resolution can be obtained with up to about a fourfold zero fill. Zero-filling is mathematically equivalent to interpolation and adds no new information – neither signal nor noise. Its only cost is digital memory and processing time.

Given the signal's approximately exponential decay with time t during the acquisition window while the r.m.s. noise remains constant, it also makes sense to match the corresponding decline in SNR with a filter that reduces the noise at the same rate. Multiplication of the time-domain signal by an exponential filter, $\exp(-t/T_{\mathrm{f}})$ whose time-constant, T_{f}, matches the signal decay, $T_2{}^{\star}$, is another standard MRS practice. Exponential filtering improves SNR, albeit at the expense of a broader linewidth produced by the faster decay. The decay rates are additive, so the apparent T_2-rate post-filtering is $1/T_{2\mathrm{f}} = \{1/T_2{}^{\star} + 1/T_{\mathrm{f}}\}$. From equation (17) after filtering the f.w.h.m. is $\{1/(\pi T_2{}^{\star}) + 1/(\pi T_{\mathrm{f}})\}$. Gaussian filtering may be performed with a function $\exp\{-\pi(t/2T_{\mathrm{f}})^2\}$ to match T_{f} to T_2 consistent with the time-domain conjugate of equation (19), $f_{\mathrm{G}}(t) \sim \exp\{-2(\pi\sigma t)^2\}$. The filter settings are conventionally reported as rates, $1/T_{\mathrm{f}}$ in hertz.

NMR Spectroscopy

Chemical Shift

Many of the earliest NMR experiments were designed to measure the gyromagnetic ratios (γ's) of the nuclei. However, as B_0 homogeneity and the spectral resolution of NMR spectrometers improved, it was found that the same nuclei on different molecular compounds resonated at slightly different frequencies.[20,21] The effect was attributed to the fact that nuclei experience not exactly the main externally applied magnetic field, but the net local field after it is screened or shielded by the electrons that surround the nucleus. This shielding arises from the effect of B_0 on the electron's motion, which produces a small magnetic field that opposes B_0 (analogous to Lenz's law). The effective field at the nucleus is

$$\mathbf{B}_{\mathrm{eff}} = \mathbf{B_0}(1-\sigma) \qquad (26)$$

where σ is called the 'shielding constant'. Consequently, the NMR frequency is shifted to

$$\nu = \gamma \mathrm{B}_{\mathrm{eff}} = \gamma \mathrm{B}_0(1-\sigma) = \nu_0(1-\sigma) \qquad (27)$$

This frequency shift is known as the *chemical shift*.

In equation (27), ν_0 is now the resonant frequency of the bare nucleus – in theory. In practice, it is the frequency of an agreed upon reference compound. For ^{1}H and ^{13}C NMR, the reference resonance is tetramethyl silane (TMS); for ^{31}P NMR, it is phosphoric acid ($\mathrm{H_3PO_4}$) in vitro or phosphocreatine (PCr) in vivo. The chemical shift is customarily defined as the difference in resonant frequency from the reference, measured in 'parts-per-million (p.p.m.)' relative to ν_0,

$$\delta = (\nu_0 - \nu)\cdot 10^6/\nu_0 \qquad (28)$$

displayed with δ increasing to the left ($-x$-axis). *Because σ is not field dependent, neither is δ.* However, because $\nu = \gamma \mathrm{B}_{\mathrm{eff}}$, the magnitude of the chemical shift dispersion, $\{\nu_0 - \nu\}$ measured in hertz, increases linearly with B_0. Consequently, *the spectral resolution of an NMR spectrum also increases linearly with*

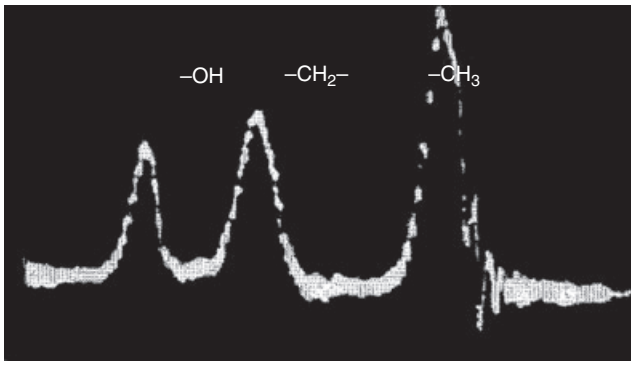

Figure 8. Perhaps the first NMR spectrum of an organic compound published.[21] This ^{1}H spectrum from ethanol recorded at 0.76 T shows the three moieties (–OH, $-CH_2-$, and $-CH_3$) as a function of field strength, with the –OH and $-CH_2-$ groups separated by about 1.6 μT or 2 p.p.m. (Reprinted with permission from J. T. Arnold, S. S. Dharmatti, and M. E. Packard, J. Chem. Phys., 1951, 19, 507. Copyright 1951, AIP Publishing LLC)

B_0, provided that the linewidths (or T_2s) are not frequency dependent.

The chemical shift phenomenon has proven immensely valuable in chemistry and biochemistry, because the same groups of magnetically equivalent nuclei or 'moieties' in different chemical environments can be distinguished and identified based on their resonant frequencies. One of the earliest examples is pictured in Figure 8.[21] This c.w. NMR spectrum of ethanol revealed ^{1}H resonances from its three moieties, $-CH_3$, $-CH_2-$, and –OH, in characteristic locations with relative intensities 3 : 2 : 1 corresponding to the relative nuclear spin densities, n_m, of protons on each moiety, on the molecule.[21] *The chemical shift effect requires a chemical (electron) bond, and does not occur through space (hydration or hydrogen bonds do not qualify). In general, the relative peak areas from each moiety are proportional to the number of NMR nuclei on the moiety.* Because relaxation is intimately associated with the local molecular-level environment, which can vary with position and the degrees of freedom of mobility on the molecule, *each moiety can have its own separate T_1 and T_2*, and often does.

Note that, strictly speaking, σ is a tensor that depends on the orientation of the molecule relative to $\mathbf{B_0}$. However, for molecules in liquid-like phases, as in most in vivo applications, σ may be considered a scalar. Early attempts at calculating σ from the effect of electron shielding currents on nuclei in magnetic fields decomposed it into a sum of paramagnetic and diamagnetic terms that were linked to the symmetry of electronic orbitals, interactions with neighboring atoms, and interatomic currents.[22,23] While differences in the paramagnetic contribution provided some insights into the large chemical shift ranges seen in nuclei such as ^{19}F (~300 p.p.m.), ^{31}P (~40 p.p.m. in vivo), and ^{13}C (~200 p.p.m. in vivo), as compared to ^{1}H (~10 p.p.m. in vivo), in practice, the complexity and sheer number of chemical interactions render such computations far less useful than the few seconds it takes to perform an actual NMR spectroscopy experiment. Chemical shift ranges for some common ^{1}H moieties are depicted in Figure 9.

Spin–Spin Coupling

In striving to further improve the NMR spectroscopy experiment with yet more homogeneous magnets to achieve narrower resonance linewidths and therefore higher SNR, it was found that not only did NMR spectra consist of individual lines for each moiety, but that each moiety itself often split into groups of lines, or 'multiplets'.[24] The multiplet structure arises from interactions involving 'spin–spin coupling' between nuclei that cause energy levels to split, resulting in several transitions instead of the single transition otherwise expected. The interactions responsible for spin–spin coupling are *intramolecular: acting only through electron bonds, and not through space.* These are not to be confused with spin–spin coupling involving dipole–dipole interactions that can be intermolecular, but often average to near zero for small molecules in solution.

Consider two spin-1/2 nuclei, A and B, with A parallel to $\mathbf{B_0}$. An electron near A will tend to orient antiparallel to A. Another electron in the same orbital will be antiparallel to the first electron (by the Pauli exclusion principle), and therefore parallel to A. If the second electron is near B, it will tend to orient B, thereby communicating information about the spin orientation of nucleus A to nucleus B. The most favorable state is when nuclei A and B are antiparallel. When A flips during NMR, its transition energy depends on the initial orientation of B relative to A, giving rise to two spectral lines. The difference in frequency corresponding to the energy difference is proportional to the interaction or coupling between A and B, and is called the 'coupling constant, J', measured in hertz. Coupling can occur when two nuclei are

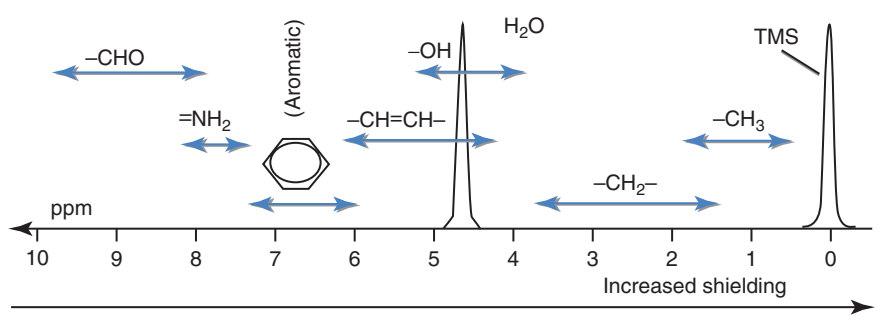

Figure 9. ^{1}H chemical shift ranges (horizontal arrows) for some common organic moieties (TMS = tetramethyl silane)

bonded together or when several bonds intervene, although the magnitude of the coupling tends to decrease as the number of intervening bonds increases. *Coupling can be between the same nuclear isotopes – termed 'homonuclear coupling' – or between different NMR nuclei – called 'heteronuclear coupling'. Importantly, J, in hertz, is independent of B_0.*

Spin–spin coupling in spectra arising from nuclei of the same type is commonly treated by a first-order analysis when (i) the chemical shift difference between nuclei or groups of nuclei is much larger than the spin coupling between them and (ii) the nuclei on a coupled group or moiety are both chemically and magnetically equivalent. Nuclei are chemically equivalent when they have the same chemical shift, and magnetically equivalent when they are of the same isotope, coupled equally with any other single nucleus in the molecule. Under these conditions, the number of peaks in a multiplet, their spacing, and their relative intensities follow the following rules:

1. A nucleus or moiety coupled to another moiety comprised of a set of n_m nuclei with spin I, will have a multiplet of $\{2n_mI+1\}$ lines.
2. The relative intensities of the $\{2n_mI+1\}$ lines are determined from the number of ways each spin state (aligned with or against B_0 etc.) can be formed. For $I=1/2$ (e.g., ^1H, ^{31}P, and ^{13}C), the relative intensities of the $\{n_m+1\}$ lines correspond to the coefficients of a binomial series (Table 2).
3. The $\{2n_mI+1\}$ lines are equally spaced and separated by J, the coupling constant.
4. Coupling between magnetically equivalent nuclei within a moiety does not affect the spectrum.

When condition (i) is not met, the spectrum may be strongly coupled or 'second order'. In this case, multiplet symmetry may be lost, the spacing may not equal J, and the splittings and multiplets may no longer correspond to a single moiety. Computer simulations may aid spectral assignment.

The rules are applied by assuming the viewpoint of each moiety in turn, treating all nuclei on the moiety you are on as one. For example, consider the case of homonuclear ^1H spin–spin coupling in acetaldehyde (CH_3CHO), which has two moieties, CHO and CH_3 (Figure 10a). All the CH_3 protons are magnetically equivalent and have a single chemical shift. From the CH_3 moiety proton's viewpoint (Figure 10b), there is a carbon bond that has a 98.9% isotopic probability of being a ^{12}C with no nuclear spin, and a single proton (^1H) on the CHO group. The 99.96% abundant ^{16}O isotope also has no spin. Thus, from Table 2, $n_m=1$ and the CH_3 is split into a doublet with equal peak intensities that correspond to the two possible spin alignments of the CHO proton, with and against B_0. Now from the CHO's viewpoint, there are $n_m=3$ proton nuclear magnets on the other side of the carbon bond. Therefore, the proton on the CHO group is split into a quadruplet with relative amplitudes 1 : 3 : 3 : 1. This arises from the $2^3=8$ combinations that three protons can be oriented with and against B_0 (one combination each with all spins oriented either with or against B_0 and three combinations each with two of three spins oriented either with or against B_0 (Figure 10a)). Finally, because there are three protons on the CH_3 and only one on the CHO, the integrated signal of the doublet is three times the integrated signal from the quadruplet.

Heteronuclear spin–spin coupling is illustrated in the case of difluoromethane (CH_2F_2; Figure 10c). The ^{19}F nucleus has 100% isotopic abundance, has a strong nuclear magnetic moment, and is chemically bonded to the same carbon. If this

Table 2. Number of multiplet peaks and relative intensities in spin–spin coupled spectra

n_m	Number of peaks in multiplet	Relative intensities
0	1	1
1	2	1, 1
2	3	1, 2, 1
3	4	1, 3, 3, 1
4	5	1, 4, 6, 4, 1, etc.

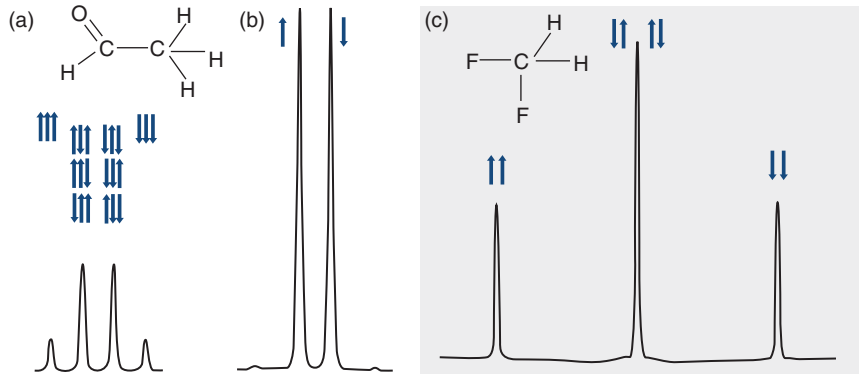

Figure 10. (a, b) Acetaldehyde has two ^1H-bearing moieties, –CHO and CH_3. (a) The –CHO moiety is split into a 1 : 3 : 3 : 1 multiplet corresponding to the number of energetically different orientations of the three spins on the CH_3 group (blue arrows: all up, all down, three combinations with two spins up, and three combinations with two spins down). (b) The $-CH_3$ moiety is split into a doublet from the two possible orientations of the proton on the –CHO group (up or down). The integral of the doublet is 3× that of the quadruplet. (c) Difluoro-methane has two magnetically different moieties of two spins each, giving rise to a 1 : 2 : 1 triplet in ^1H and ^{19}F spectra arising from the three different spin combinations (all up, all down, and two combinations with one spin up and one down)

were regular methane (CH_4), all the protons would be indistinguishable and constitute a single moiety with a single peak. However, two ^{19}F nuclei cannot be magnetically equivalent to two ^{1}H nuclei. The H_2 and F_2 therefore behave as two moieties, each split by the other into a single triplet in the ^{1}H spectrum and also in the ^{19}F spectrum. The triplets have amplitudes 1 : 2 : 1 corresponding to $n_m = 2$.

Decoupling and Overhauser Enhancement

While spin–spin coupling provides information on the chemical structure of adjacent chemically shifted moieties, in applications of MRS to materials comprised of mixtures of substances such as biological tissues, the presence of overlapping multiplet structures can obfuscate the identification and quantification of metabolites and/or compounds of interest. In addition, dividing up the NMR signal from a moiety into multiple peaks reduces the SNR relative to having the entire signal concentrated in a single peak. Fortunately, it is possible to collapse the multiplet structure of a moiety A that arises from its spin–spin coupling to a neighboring moiety B, into a single line. This is achieved by applying a second 'decoupling' B_1 magnetic field precisely tuned to moiety B, in addition to the regular MRS excitation field. Spin decoupling of moiety A occurs when moiety B changes its alignment relative to $\mathbf{B_0}$ (i.e., flips between its multiplet energy states) at a rate faster than the coupling constant J_{AB} between A and B. This results in saturation of the multiplet states. Decoupling simplifies the spectrum of A and increases its SNR by the sum of the heights of the collapsed multiplet peaks.

When A and B are of the same isotope, the technique is called 'homonuclear decoupling'. Practical difficulties in implementing it in vivo include ensuring that the decoupling B_1 field is precisely tuned to moiety B and does not clip moiety A, especially when B_0 and ν_0 vary relative to the chemical shifts and/or linewidths of A and B over the large sample volumes encountered in vivo. The power requirements for achieving complete decoupling and protecting the NMR spectrometer's sensitive preamplifier from the decoupling power are other considerations.

When A and B are different nuclei or isotopes (e.g., ^{1}H and ^{13}C or ^{19}F), the decoupling is said to be 'heteronuclear'. Here the resonances are typically far enough away (i.e., many megahertz), that the selection of B can be 'broadband'. Broadband decoupling ensures not only the decoupling of B from A on a single 'moiety of interest' (MOI) but also the decoupling of all other B nuclei from type A nuclei, on all moieties. From the practical standpoint, all that is required is some RF filtering applied at B's NMR frequency, to stop the B_1 decoupling signal from affecting detection of A at the spectrometer's preamplifier input.

The 'Overhauser effect' is a method of transferring magnetization of one spin system – originally unpaired electrons in metals – to another spin system, via dipole–dipole interactions.[25,26] Although far less effective than 'hyperpolarization' techniques (see ***Hyperpolarization Methods for MRS***, ***Dynamic imaging of hyperpolarized ^{13}C combined with isotopomer methods to provide a comprehensive picture of metabolism***, and ***Hyperpolarized Carbon-13 MRI and MRS Studies***), the 'nuclear Overhauser effect (n.O.e.)' is primarily used in vivo for transferring polarization from a high-γ nucleus B, such as ^{1}H, to a low-γ nucleus A, such as ^{13}C, for the purpose of enhancing the SNR of the latter. An n.O.e. can be observed when dipole–dipole interactions between A and B represent a prominent T_1 relaxation mechanism for A. Basically, nucleus B is irradiated to saturation, which equalizes the spin populations in its nuclear energy levels. The spin population and transitions for A, being dipolar coupled, are also altered proportional to the ratio of γ_B/γ_A depending on the strength of the dipolar interaction [equation (3)]. The n.O.e. can be positive or negative depending on the sign of μ, and decreases as A–B dipolar interactions lessen. The maximum achievable n.O.e. is $\{1 + \gamma_B/2\gamma_A\}$. The maximum n.O.e. achievable by irradiating ^{1}H during ^{13}C MRS, for example, is $\{1 + \gamma_{1H}/2\gamma_{13C}\} = 3$.

Unlike spin–spin coupling, n.O.e. can occur through space and via intramolecular processes: it does not require a chemical bond. The n.O.e. irradiation can be turned off for periods that are short compared to T_1, such as during an acquisition window, without a significant loss in enhancement. Conversely, the decoupling irradiation must be on *during* signal acquisition to achieve spin–spin decoupling, but not necessarily *on* at other times. Figure 11 illustrates the combined effect of decoupling and n.O.e. on a ^{13}C spectrum from a human leg in vivo at 1.5 T.[27]

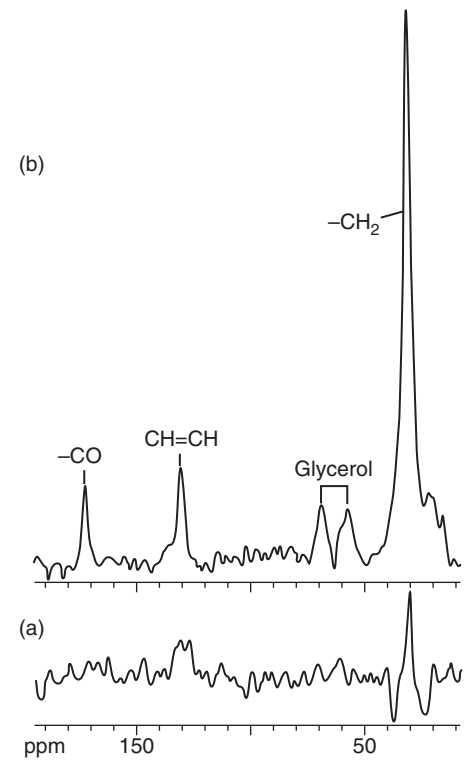

Figure 11. Natural abundance ^{13}C NMR spectrum acquired at 1.5 T by placing a loop detector coil on the leg of a healthy human volunteer without (a), and with (b) ^{1}H decoupling and n.O.e.[27] Two FIDs were averaged (TR = 0.5 s) and the decoupler deposited 3 W of RF power into the tissue. Chemical shift is relative to TMS. (Reproduced with permission from Ref. 27. © John Wiley & Sons, Ltd., 1989)

Water Suppression

^{1}H NMR spectra of solutions such as milk, wine, tissue extracts, or tissues including blood, muscle, brain, etc. are often dominated by the signal from a single component – water. This can interfere with the detection and quantification of signals from metabolite MOIs when the dynamic range of the NMR receiver is limited, when their concentrations are <0.1% of water, and/or when they are obfuscated by broad side-wings or intense motion artifacts propagating from the water signal. Signal from mobile lipid ($-CH_2-$ and $-CH_3$) moieties from fat can also be problematic in ^{1}H and ^{13}C spectra.

The problem is countered by 'solvent suppression,' 'water suppression,' and fat suppression or 'fat saturation' techniques that include the following.

T_1 Discrimination. The spectroscopy sequence is preceded by an inversion pulse applied at time TI equal to 0.693 times the T_1 of the water or lipid resonance to be suppressed, in accordance with the T_1-null method (see section titled 'T_1 and Inversion Recovery'). Note that the MOI signal will also be modulated according to equation (14) and its own T_1s.

T_2 Discrimination. If the unwanted resonances have shorter T_2s than the moieties of interest they can be suppressed with a long-TE SE sequence (see section titled 'T_2 and Spin-Echoes'). Note that the MOI signals will also be attenuated by their own T_2s via the factor $\exp(-T_2/\mathrm{TE})$.

Chemical-selective Irradiation of the Unwanted Peak. In the homonuclear decoupling experiment (see section titled 'Decoupling and Overhauser Enhancement'), an unwanted coupled resonance was eliminated by applying a B_1 field precisely tuned to saturate the resonance. The same saturation technique can be used to eliminate any undesirable peak in the spectrum. The simplest approach is a low-level c.w. B_1 signal applied throughout the experiment. Because saturation depends on T_1, B_1 can be turned off during acquisition if $\mathrm{tAQ} \ll T_1$ of the peak being suppressed, to avoid interactions between the c.w. transmission and reception.

Applying c.w. RF for more than several tens of milliseconds can be problematic for performing MRS on modern MRI scanners whose RF transmitters are often limited to short intense pulses. However, because the FT of a square excitation band in frequency space is equal to a 'sinc pulse' of the form $\mathrm{sinc}(t) = \sin t/t$ in the time domain, applying a sinc-modulated RF pulse whose excitation frequency is centered on the undesired resonance can selectively excite a square frequency band with the undesired resonance at its center. In practice, the sinc function, which is infinite with decaying sidelobes symmetrically displaced about an intense central lobe, must be truncated – usually at a zero crossing. A symmetric $\mathrm{sinc}(n\pi t/\tau)$-modulated RF pulse truncated to a total of n zero crossings (including the two ends) has a total of $\{n-1\}$ positive plus negative lobes, a central lobe of duration $2\tau/n$ (zero-to-zero crossing) and excites an f.w.h.m. BW of $\Delta\nu = n/\tau$ for $\alpha \leq 90^\circ$.[28] $\Delta\nu$ must generally be adjusted to avoid excitation of the MOI.

In the strict sense, in order to 'saturate' the unwanted resonance, the pulse must be applied for periods longer than T_1. A simpler approach is to apply just one-to-three of these prepulses before regular MRS excitation with an FA $= \alpha^\circ$ pulse. The FAs of the chemical-selective pulses are adjusted so that the unwanted resonance generates no transverse magnetization. For example, with just a single suppression prepulse of FA $= \{180^\circ - \alpha^\circ\}$, the unwanted resonance will be inverted after the α° pulse is applied. It thus can contribute no M_{xy}. Meanwhile, the MOI signal is left untouched.

The sinc function is only one of many modulation functions that can be used to modulate RF pulses for the purpose of selectively exciting limited portions of an NMR spectrum. For example, a symmetric pulse of duration τ modulated by a Gaussian function of form $f_G(t) \sim \exp\{-2(\pi\sigma t)^2\}$ [the FT conjugate of equation (19)] truncated at ~10% of its amplitude excites a Gaussian-shaped band in the frequency domain with an f.w.h.m. of about $1.14/\sqrt{\tau}$ Hz,[28] or 36 Hz for a 1 ms pulse. Even the conjugate of the sinc pulse, the simple square-modulated time-domain pulse of duration τ used extensively in earlier sections, has a finite bandwidth: a sinc-modulated frequency response with an f.w.h.m.[28] of $1.21/\tau$. This must be remembered when using them for exciting large chemical shift dispersions.

Chemical-selective Excitation of the MOIs. The converse version of the method in the last section titled 'Chemical-selective Irradiation of the Unwanted Peak', is to avoid exciting the unwanted resonance at all. In this case, the center frequency of the selective excitation pulse, say an α° sinc-modulated RF excitation pulse, is shifted and its excitation width adjusted to accommodate the BW of the spectrum of interest. Portions of the spectrum lying outside of the excitation window are unexcited, and therefore suppressed accordingly. Because the region of interest is now directly excited by the chemical-selective excitation pulse and hence is modulated by its excitation spectrum, unmodulated square or Gaussian pulses are far less desirable than sinc and related tailored pulse modulations from the standpoint of introducing spectral distortion.

NMR Filtering Employing Selective Spin Coupling or Editing. The T_1 relaxation and coupling properties of nuclear spins can also be used to target and distinguish an MOI from background signals that do not participate in such coupling. Typically, the NMR signal from the MOI is observed with and without selective NMR irradiation of the moiety that is coupled to it, analogous to homonuclear decoupling in the section titled 'Decoupling and Overhauser Enhancement'. This is primarily used for targeting moieties on specific metabolites against a background milieu of other metabolites and will be treated later under 'spectral editing' (see ***Spectral editing in MRS***).

Signal-to-Noise Ratio (SNR)

Definition and Dependencies

The SNR is arguably *the* most critical determinant of NMR success. In MRS, it is defined as the signal height of the absorption mode (in-phase) component of the circularly polarized signal, divided by the r.m.s. noise (see section titled 'Circular Polarization of B_1'), as detected by the NMR spectrometer. Signal height, S_p, is actually the easier of the two to measure, the main

complication being the determination of the baseline offset, S_b, at the location of the peak, in the presence of rolling baseline artifacts or overlapping resonances that are all too common in vivo. The r.m.s. noise, ν_n, must be determined from a region of spectrum devoid of signal and baseline artifacts and is preferably acquired with the sample in the spectrometer using the same settings as for S_p, but with the excitation turned off. At the very least, when determining signal and noise from the same spectrum spectral artifacts must be removed otherwise the true SNR can easily be underestimated manyfold. If the mean of the noise $\overline{\nu_n} \neq 0$ is offset, it should be subtracted from ν_n as well. Thus,

$$\mathrm{SNR} = \frac{(S_p - S_b)}{(\nu_n - \overline{\nu_n})} \tag{29}$$

A rough estimate of SNR also obtains by taking 2.5 times the peak height divided by the maximum peak-to-peak variation in the noise.

The SNR depends on the MOI concentration, the strength and homogeneity of the main field B_0, NMR pulse sequence parameters such as signal averaging (signals add $\propto N$ while random noise adds $\propto \sqrt{N}$: see section titled 'Fourier Transform NMR'), receiver BW setting, and other instrumental factors in accordance with Table 3.[1,29–32]

Calculation of SNR

Modern numerical methods make the calculation of absolute SNR possible.[32,33] The computation relies on the 'Principle of Reciprocity', which relates the sensitivity of a detector to a small subvolume ΔV of magnetic dipole sources at some location p, to the signal detected at p when a virtual unit current is applied to the coil.[29,1] From Faraday's Law applied to $M(t) \sim \exp(i\omega_0 t)$ from the section titled 'Fourier Transform NMR', the signal voltage is:

$$S(t) = \mathrm{d}\{\mathbf{M} \cdot \mathbf{B_{10}} \Delta V\}/\mathrm{d}t = \omega_0 M \cdot |B_{10}| \Delta V \tag{30}$$

where $|B_{10}|$ is the magnitude of the circularly polarized transverse magnetic field $\mathbf{B_{10}}$, generated by the detector excited with unit current [analogous to equation (7)].

The noise voltage is given by the Nyquist formula[34]:

$$\nu_n = \sqrt{4KTR_L\mathrm{BW}} \tag{31}$$

where R_L is the resistance of the detector loaded with the sample at $\omega_0 \cdot R_L$ is usually decomposed into contributions from the sample and detector coil, $R_L = R_{coil} + R_{sample}$. T is the temperature of the load's dominant noise source. At equilibrium, the ^{1}H nuclear magnetization of a milliliter of water in a field of B_0 tesla at 37 °C (310 K) is[1]

$$M_0 = N_{ml}\nu_0^2 h^2 I(I+1)/3\,\mathrm{KT} = 3.111 \times 10^{-9} \times \mathrm{B_0\,J \cdot T^{-1} \cdot ml^{-1}} \tag{32}$$

Dividing equation (30) by (31), the SNR per milliliter is thus:

$$\mathrm{SNR} = \frac{\sqrt{2}\omega_0 M|B_{10}|}{\sqrt{4KTR_L\mathrm{BW}}} \times 10^{-\frac{\mathrm{NF}}{20}} \tag{33}$$

with the $10^{-\mathrm{NF}/20}$ term added to account for losses in the NMR spectrometer, as indexed by the NMR system's noise figure (NF) measured in decibel.[31] The $\sqrt{2}$ accounts for the circular polarization of the NMR signal (see section titled 'Circular Polarization of B_1'), and is removed for linear detectors.[32]

Solving equation (33) boils down to calculating $|B_{10}|$ and $\sqrt{R_L}$, as the rest of the equation involves substituting constants, and any differences between M and M_0 due to the various NMR pulse sequences are easily accommodated via equations (8), (9), (12), (14), (16), etc. $|B_{10}|$ is fairly easily calculated from the NMR detector's known current conductor locations and Biot–Savart's law, for example.[35] Typically, R_L is determined numerically for the ideal case of negligible system noise (NF = 0) and coil noise ($R_{coil} = 0$), based on the RF electrical properties of the sample (conductivity σ; dielectric constant ε) using:

$$R_{sample} = \sigma \int_{sample} |E(r)|^2 \mathrm{d}V \tag{34}$$

where $|E(r)|$ represents the magnitude of the RF electric field generated by unit current, which is integrated over the sample volume V. Commercial numerical electromagnetic (EM) software engines are available to perform both the $|B_{10}|$ and R_L computations by breaking up the volume into tiny elements to solve discretized versions of Maxwell's equations.[32,33]

The SNR that obtains for the 'ideal detector' with negligible system and coil noise is called the 'intrinsic signal-to-noise ratio' or 'ISNR', as it is attributable to sample losses only. This is the best possible SNR realizable for the chosen configuration of coil or detector conductors.[31] However, the application of such software engines can be extended to determine the 'ultimate intrinsic signal-to-noise ratio (UISNR)'.[36] Basically, the locations of the current sources that generate $|B_{10}|$ are iteratively adjusted on the surface of a model sample, to numerically optimize the SNR in a region of the sample. The UISNR is the best SNR that can be obtained by any coil design.[36]

Detectors and B_0 Dependence

Obviously, detector performance plays a key role. Generally, it is desirable to localize the MRS signals to subvolumes, ΔV, of interest in the sample using methods such as those described in later chapters. Because the detector receives both signal and noise voltages without discrimination, an optimal detector should primarily be spatially sensitive only to the signal and the

Table 3. Dependence of SNR on experimental and detection system parameters

Parameter	Number of nuclei (V, ml)	B_0 strength (T)	B_0 uniformity (p.p.m.)	Averages, N	BW	Coil size, a	Loaded coil Q_L	Noise figure NF (in dB)	Temperature, T (in K)
SNR varies as:	Linearly	B_0^1 to B_0^2	~Linearly	$\sqrt{N}$	$1/\sqrt{\mathrm{BW}}$	$\sim a^{-3/2}$	$\sqrt{Q_L}$	$10^{(\mathrm{NF}/20)}$	$1/\sqrt{T}$

noise from ΔV and not detect extraneous noise from regions outside of ΔV. This argues for detector coils whose dimensions are matched to the location and size of the subvolumes, such as loop detectors with diameters about equal to the depth and extent of interest.[33,35]

The detector should contribute negligible thermal electrical noise to the spectrum from its own resistive losses.[29,30] The detector is invariably tuned via a resonant circuit to the NMR frequency, ν_0, in order to maximize the amplitude of the induced signal voltage that is conveyed to the NMR spectrometer's voltage preamplifier. The coil's unloaded quality factor, $Q_E = \{\omega L/R_{coil}\}$, is a measure of the coils own resistive losses, as well as the sharpness of the resonant circuit. The tuning circuit also matches the resistance of the detector at resonance, to the input impedance of the preamplifier at which its NF is minimum, using minimal-loss reactive elements (see ***Magnetic Resonance Spectroscopy Instrumentation***).

When a biological sample – a human subject, animal, a biological sample, etc. – is placed in the coil, the quality factor, Q, decreases to $Q_L = \{\omega L/R_L\} = \{\omega L/(R_{coil} + R_{sample})\}$.[30] For the ideal detector then, $Q_L \ll Q_E$. However, caution is necessary. A low Q_L or high R_L is detrimental to SNR regardless (Table 3) and can also arise from unnecessary direct electrical coupling between the detector and the sample in nonideal designs. This is often manifest as changes in the detector's resonant frequency when it is loaded with the sample, and such losses can often be ameliorated by superior detector design such as those that distribute the tuning elements throughout the detector's structure.

The Intrinsic SNR. Equation (33) contains several factors whose B_0 dependence must be parsed when considering the SNR benefits of higher NMR field strengths. On the signal side, replacing ω_0 in equation (30) by$\{\gamma\ B_0\}$ from equation (1) and noting $M \propto B_0$ as well [see section titled 'Exciting Resonance' and equation (32)], we have $S(t) \propto {B_0}^2$. Then, from equation (31) for the noise,

$$\mathrm{SNR} \propto \frac{{B_0}^2}{\sqrt{R_L}} = \frac{{B_0}^2}{\sqrt{R_{coil} + R_{sample}}} \qquad (35)$$

For external detectors, R_{coil} is proportional to the reciprocal of the RF skin depth,[27,28] $\delta = \{2\rho/(\mu_c\omega_0)\}^{1/2}$ for a coil made of conductor of resistivity ρ and permeability μ_c. Thus, $R_{coil} \propto \sqrt{\omega_0}$. The losses contributing to R_{sample} in equation (34) are primarily inductive[30,31] and vary as ${\omega_0}^2$. Therefore, after converting the R dependencies in ω_0 into B_0 dependencies, equation (35) becomes:

$$\mathrm{SNR} \propto \frac{{B_0}^2}{\{(1 - a_c){B_0}^2 + a_c{B_0}^{1/2}\}^{1/2}} \qquad (36)$$

where a_c is introduced as a measure of the fraction of the noise contributed by the detector.[30,31] The case of $a_c = 0$ corresponds to the ideal zero-noise detector with SNR equal to the ISNR, which scales only linearly as B_0 (Figure 12).[31] If $a_c = 1$, coil noise is dominant and SNR scales as $\sim {B_0}^{7/4}$ (Figure 12).[29]

Caution is warranted when using equation (36) to predict performance at one B_0 based on the SNR measured at another. The expression is a proportionality so everything else must

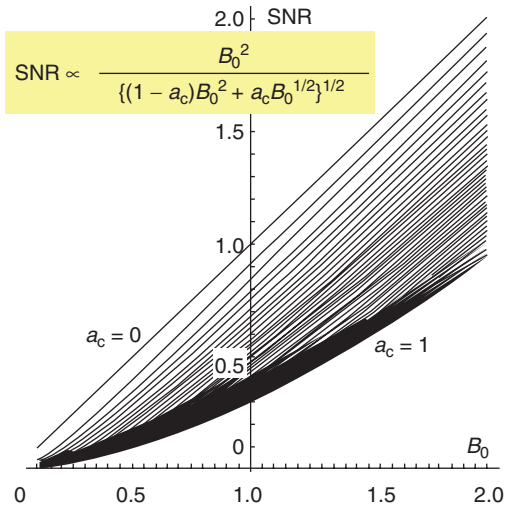

Figure 12. Dependence of SNR on B_0 according to the proportionality of equation (36), as a function of the relative contributions to the noise from the sample and the coil ($0 \le a_c \le 1$; 2% steps; arbitrary units)

be the same for any comparison: this means BW, coil design, coil size, B_0 homogeneity, pulse sequence parameters, etc. In addition, coil designs optimized for one B_0 may be ill-suited for another B_0, especially if the comparison involves a large difference in B_0. For example, the change from 0.3 to 1.5 T prompted the invention of the birdcage coil.[12] In addition, as coil size is reduced to improve SNR by minimizing the noise detected from remote locations (*a* in Table 3), it becomes increasingly difficult to achieve the sample-dominant noise condition because relative losses in coil conductors, solder joints, and tuning capacitors mount.[37] Although one is rewarded by $a \sim {B_0}^{7/4}$ SNR dependence, the SNR gained from operating in the coil-noise dominant 7/4th power regime is still less than what it would be without the coil noise (Figure 12). An extreme case perhaps is that of tiny internal coils that employ the body as a return path.[32] These can behave like antennae in lossy media whose noise is dominated by sample electrical losses. In this case,[32] R_L in equation (35) may be essentially constant with B_0, resulting in an SNR $\propto {B_0}^2$ as the best that can possibly be done for the design, but less than the UISNR that would result without these losses.[38]

Because the change in Q_E and Q_L is a measure of the change in the relative load resistances in equation (35), the ISNR can be determined from a regular SNR measurement via:

$$\mathrm{ISNR} = \frac{\mathrm{SNR} \cdot 10^{\mathrm{NF}/20}}{(1 - Q_L/Q_E)^{1/2}} \qquad (37)$$

with the NF term accounting for losses in the NMR spectrometer as in equation (33).[31] In practice (and detailed more generally in ***Magnetic Resonance Spectroscopy Instrumentation***), NF can be measured by replacing the NMR coil by a thermally stable 50 Ω resistor at the system's preamplifier input, and acquiring a spectrum at room temperature (RT), with no RF excitation.[39] A measurement of ν_{nRT} is made from the unfiltered spectrum. The resistor is dunked in liquid nitrogen at $T = 77$ K, and the noise measurement repeated to obtain ν_{n77}.

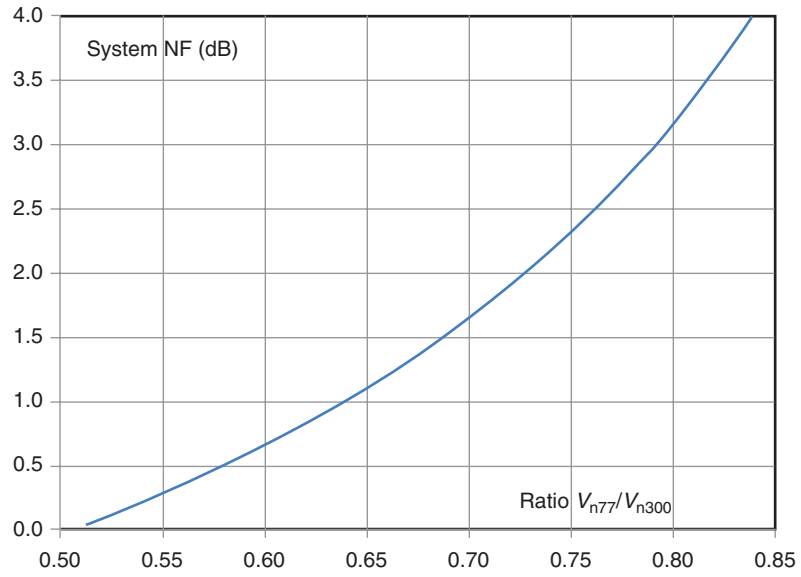

Figure 13. Measurement of the system noise figure (NF) from the ratio of noise voltages from a 50 Ω resistor in liquid nitrogen to that at 300 K (27 °C), at the system's preamplifier input, according to equation (38) for ratios of about 0.5–0.85[39]

Basically, the larger the decrease in v_{n77}, the more sensitive the scanner is to thermal noise – in this case, the resistor's noise – and the lower the NF. NF at *RT* may be calculated from[1]

$$\mathrm{NF} = 10\log[1 - 77/\mathrm{RT}] - 10\log[1 - (v_{\mathrm{nRT}}/v_{n77})^2], \quad (38)$$

the plot in Figure 13,[39] or the more generalized form of equation (13) given in ***Magnetic Resonance Spectroscopy Instrumentation***.

SNR Limits In Vivo

The primary factor limiting SNR in vivo is the concentration of the chemical moiety, or N_{ml}. As already noted (see section titled 'Eligible Nuclei'), ^{1}H nuclei far outnumber other nuclei in living tissue, amounting to about two-thirds of them. About two-thirds of the protons are in endogenous water moieties,[2] whereas the rest of the protons mostly reside in various organic molecules that make up the body. Of the latter, fat is probably the most abundant, accounting for perhaps 22% of the proton pool.[2] Then, there is a *sensitivity gap* between the water and fat signals and those of other MOIs detectable by ^{1}H NMR, which are present at much lower concentrations. The current limit to practical detection by NMR or MRS is about 10^{-6} of that of ^{1}H signal from water. Most endogenous metabolites that are NMR-visible are in the 1–10 mM concentration range: about $\sim 10^{-5}$ of that of ^{1}H in water. Non-^{1}H NMR is further compromised by reduced sensitivity, isotopic abundance, and SNR relative to ^{1}H (Table 1). One may query how can they be seen at all? The answer draws on Table 3. The SNR for tissue water ^{1}H is of the order 100 $\sqrt{\mathrm{Hz}}/\mu$l per FID. Averaging 100 FID's from a much larger volume–say 10 ml (vs 1 μl), and reducing BW 16-fold can more than compensate for the loss (since $10^4\sqrt{\{100 \times 16\}} = 4 \times 10^5$).

Note that highly bound substances such as membrane lipids with short T_2s (or very broad linewidths) whose signals have decayed by the time of the acquisition window will be 'NMR invisible'. In addition, NMR or MRS can be performed on nonendogenous compounds containing NMR nuclei such as fluorine (^{19}F), or ^{13}C-enriched compounds, including those that are hyperpolarized (see ***Hyperpolarization Methods for MRS***, ***Dynamic imaging of hyperpolarized ^{13}C combined with isotopomer methods to provide a comprehensive picture of metabolism***, and ***Hyperpolarized Carbon-13 MRI and MRS Studies***). However, our ability to see hyperpolarized nuclei will still depend on what concentration can be introduced, as well as how much hyperpolarization is retained.

What can be seen in vivo with MRS will be reviewed in forthcoming chapters and appendices, but here is a brief preview.[40]

Fat and Lipid Metabolism. Fatty acids with $-CH_2-$ resonances are sufficiently concentrated to be imaged directly by 'chemical selective' ^{1}H MRI using techniques analogous to those discussed in the sections titled 'Chemical-selective Irradiation of the Unwanted Peak' and 'Chemical-selective Excitation of the MOIs'. They are also visible in natural abundance ^{13}C MRS (Figure 11).[27] Phospholipid membrane components such as phosphorylethanolamine and phosphorylcholine are precursors to brain myelin and appear as a phosphomonoester (PM or PME) resonance in ^{31}P spectra. Breakdown products, glycerophosphorylethanolamine, and glycerophosphorylcholine appear as phosphodiester (PD or PDE) peaks in ^{31}P MRS.

Energy Metabolism. Adenosine triphosphate (ATP) is the fundamental energy currency of the body. Short-term energy is

produced by conversion of ATP into adenosine diphosphate (ADP) and inorganic phosphate (Pi):

$$ATP^{\S} \Longleftrightarrow ADP + Pi^{\S} + \text{energy}$$

In brain and muscle (skeletal and heart), ATP is resupplied from phosphocreatine (PCr) via the creatine kinase (CK) reaction:

$$PCr^{\S} + ADP \Longleftrightarrow ATP^{\S} + \text{creatine}^{\P}$$

and also from

$$\text{Glycogen}^{\#} + Pi^{\S} + ADP \Longleftrightarrow ATP^{\S} + \text{lactic acid}^{\#\P}$$

Long term aerobic energy sources include:

$$\text{glucose}^{\#\P}, \text{glycogen}^{\#\P} + ATP^{\S} + Pi^{\S} + O_2 \Rightarrow ATP^{\S} + H_2O + CO_2$$

$$\text{fatty acids}^{\#\P} + ADP + Pi^{\S} + O_2 \Rightarrow ATP^{\S} + H_2O + CO_2$$

Glycolytic metabolism converts 1 mole of glucose into lactate to make 2 moles ATP, whereas its complete combustion via the citric acid cycle makes 36 moles of ATP:

$$\text{glucose}^{\#\P}, \text{pyruvate}^{\#\P} \Rightarrow \text{lactate}^{\#\P} + ATP^{\S}$$

$$\text{amino acids, carbohydrates, fats}^{\#\P}, \text{glucose}^{\#\P}, \text{pyruvate}^{\#} \Rightarrow \text{acetylcoenzyme A}$$

$$\text{acetylcoenzyme A} \Rightarrow \alpha\text{-ketoglutarate} \Rightarrow \text{glutamate}^{\#\P} \Longleftrightarrow \text{glutamine}^{\#\P}$$

$$\text{acetylcoenzyme A} \Rightarrow \text{oxaloacetate} \Longleftrightarrow \text{aspartate}^{\#\P}$$

Neuroexcitation and Inhibitory Metabolites. Glutamate, aspartate, and gamma-aminobutyric acid (GABA; derived from glutamate) are detectable by brain ^{1}H MRS, as is n-acetyl aspartate, whose specific biochemical function remains unclear even though it is often referred to as a 'neuronal marker'.

Biographical Sketch

Paul A. Bottomley. BSc (Hon.), 1975, PhD, 1978, Physics, University of Nottingham, UK. Research Associate, Johns Hopkins University, Baltimore, 1978–1980. Physicist, G. E. Research and Development Center, 1980–1994. Currently Russell H Morgan Professor and Director of the Division of MR Research of the Russell H Morgan Department of Radiology and Radiological Sciences, Johns Hopkins University. Fellow and Gold Medal recipient of the Society of Magnetic Resonance in Medicine, 1989; Gold Medal, American Roentgen Ray Society 2015; Coolidge Fellowship and medal, G.E. Company, 1990; Gold, Silver, and Bronze patent medals; 39 issued patents, about 180 peer-reviewed papers, 21 book chapters, 13 editorials, and over 225 published abstracts. Research specialties: in vivo NMR, MRI, tissue relaxation times, localized NMR spectroscopy, human cardiac NMR spectroscopy, interventional MRI, and MRI safety.

Related Articles

Magnetic Resonance Spectroscopy Instrumentation; Fourier Transform Spectroscopy; Spatial Localization Techniques for Human MRS; Detection coils for MRS; Carbohydrates and Glycoconjugates; Whole Body Studies Involving Spin-Lattice Relaxation in the Rotating Frame; Metabolite Quantification in MRS and Pattern Recognition; Development of NMR: Biological and Medical MR Spectroscopy; Recent Progress in Clinical Magnetic Resonance Spectroscopy; Magnetic Shielding and Chemical Shifts: Basics; Dipolar and Indirect Coupling: Basics

§Detectable by ^{31}P MRS.
¶Detectable by ^{1}H MRS.
$^{\#}$Detectable by ^{13}C-enriched MRS (including enhanced polarization methods).

References

1. C. N. Chen and D. I. Hoult, Biomedical Magnetic Resonance Technology, A. Hilger: Bristol, New York, 1989, 120, 196, 309.
2. W. S. Snyder, M. J. Cook, E. S. Nasset, L. R. Karhausen, G. P. Howells, and I. H. Tipton, Report of the Task Group on Reference Man, Pergamon Press: Oxford, 1984, 296, 326, 281 International Commission on Radiological Protection No. 23.
3. E. M. Purcell, H. C. Torrey, and R. V. Pound, *Phys. Rev.*, 1946, **69**, 37.
4. F. Bloch, W. W. Hansen, and M. Packard, *Phys. Rev.*, 1946, **69**, 127.
5. P. C. Lauterbur, *Nature*, 1973, **242**, 190.
6. E. L. Hahn, *Phys. Rev.*, 1950, **80**, 580.
7. N. Bloembergen, E. M. Purcell, and R. V. Pound, *Phys. Rev.*, 1948, **73**, 679.
8. A. Abragam, The Principles of Nuclear Magnetism, Oxford University Press: Oxford, UK, 1978, 292.
9. P. A. Bottomley, T. H. Foster, R. E. Argersinger, and L. M. Pfeifer, *Med. Phys.*, 1984, **11**, 425.
10. P. A. Bottomley, C. J. Hardy, R. E. Argersinger, and G. Allen-Moore, *Med. Phys.*, 1987, **14**, 1.
11. F. Bloch, *Phys. Rev.*, 1946, **70**, 460.
12. C. E. Hayes, W. A. Edelstein, J. F. Schenck, O. M. Mueller, and M. Eash, *J. Magn. Reson.*, 1985, **63**, 622.
13. G. H. Glover, C. E. Hayes, N. J. Pelc, W. A. Edelstein, O. M. Mueller, H. R. Hart, C. J. Hardy, M. O'Donnell, and W. D. Barber, *J. Magn. Reson.*, 1985, **64**, 255.
14. C. N. Chen, D. I. Hoult, and V. J. Sank, *J. Magn. Reson.*, 1983, **54**, 324.
15. H. Y. Carr and E. M. Purcell, *Phys. Rev.*, 1954, **94**, 630.
16. S. Meiboom and D. Gill, *Rev. Sci. Instrum.*, 1958, **29**, 688.
17. D. Burstein, *Conc. Magn. Reson.*, 1996, **8**, 269.
18. P. A. Bottomley and W. A. Edelstein, Method of eliminating spurious FID due to imperfect 180° pulses in NMR imaging: the primer/crusher sequence, U.S. Patent 4,484,138; (Nov. 20, 1984).
19. R. R. Ernst and W. A. Anderson, *Rev. Sci. Instrum.*, 1966, **37**, 93.
20. W. G. Proctor and F. C. Yu, *Phys. Rev.*, 1950, **77**, 717.
21. J. T. Arnold, S. S. Dharmatti, and M. E. Packard, *J. Chem. Phys.*, 1951, **19**, 507.
22. W. E. Lamb, *Phys. Rev.*, 1941, **60**, 817.
23. N. F. Ramsay, *Phys. Rev.*, 1950, **78**, 699.
24. H. S. Gutowsky, D. W. McCall, and C. P. Slichter, *Phys. Rev.*, 1951, **84**, 589.
25. A. W. Overhauser, *Phys. Rev.*, 1953, **92**, 411.
26. T. R. Carver and C. P. Slichter, *Phys. Rev.*, 1953, **92**, 212.
27. P. A. Bottomley, C. J. Hardy, P. B. Roemer, and O. M. Mueller, *Magn. Reson. Med.*, 1989, **12**, 348.
28. M. A. Bernstein, K. F. King, and X. J. Zhou, Handbook of MRI Pulse Sequences, Elsevier: London, 2004, 37.
29. D. I. Hoult and R. E. Richards, *J. Magn. Reson.*, 1976, **24**, 71.
30. D. I. Hoult and P. C. Lauterbur, *J. Magn. Reson.*, 1979, **34**, 425.
31. W. A. Edelstein, G. H. Glover, C. J. Hardy, and R. W. Redington, *Magn. Reson. Med.*, 1986, **3**, 604.

32. A. M. El-Sharkawy, D. Qian, and P. A. Bottomley, *Med. Phys.*, 2008, **35**, 1995.
33. J. Wang, A. Reykowski, and J. Dickas, *IEEE Trans. Biomed. Eng.*, 1995, **42**, 908.
34. H. Nyquist, *Phys. Rev.*, 1928, **32**, 110.
35. P. A. Bottomley, C. H. Lugo-Olivieri, and R. Giaquinto, *Magn. Reson. Med.*, 1997, **37**, 591.
36. O. Ocali and E. Atalar, *Magn. Reson. Med.*, 1998, **39**, 462.
37. A. Kumar, W. A. Edelstein, and P. A. Bottomley, *Magn. Reson. Med.*, 2009, **61**, 1201.
38. H. Celik, Y. Eryaman, A. Altintas, I. A. Abdel-Hafez, and E. Atalar, *Magn. Reson. Med.*, 2004, **52**, 640.
39. P. A. Bottomley, in Medical Magnetic Resonance Imaging and Spectroscopy, a Primer, eds T. F. Budinger and A. R. Margulis, Society for Magnetic Resonance in Medicine: Berkeley, CA, 1986, 81.
40. P. A. Bottomley, *Radiology*, 1989, **170**, 1.